Heliyon 10 (2024) e37411

Contents lists available at ScienceDirect

Heliyon

journal homepage: www.cell.com/heliyon

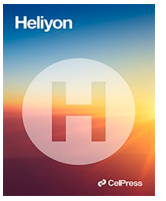

Research article

Study on vibration characteristics of the dike crossing pipeline based on EWT and CWT

Jinlin Huang [a,b,1], Ziyu Li [b,1], Jianwei Zhang [b,*]

[a] Guangdong Research Institute of Water Resources and Hydropower, Guangzhou, 510635, China
[b] North China University of Water Resources and Electric Power, Zhengzhou, 450046, China

ARTICLE INFO

Keywords:
The dike crossing pipeline
Wavelet transform
Empirical wavelet transform (EWT)
Cross wavelet transform (CWT)
Vibration characteristics identification

ABSTRACT

The dike crossing pipeline is an important part of urban water transmission and supply projects. Identifying effective vibration analysis methods to determine the primary vibration sources and coupling vibration characteristics of pipelines is crucial for targeted vibration reduction and reinforcement of vulnerable pipeline sections. Therefore, this paper proposes a coupled vibration characteristics analysis method for the dike crossing pipeline based on EWT and CWT, taking the 6# dike crossing pipeline of Yang'er water plant in Foshan city, Guangdong province as the research object, firstly, the main vibration sources of the dike crossing pipeline are analyzed with the help of the prototype observation data using the mutual correlation power spectral, and the characteristics of the main vibration sources of the pipe are extracted using the empirical wavelet transform (EWT); then, focusing on the main vibration source, wavelet transform is used to analyze the source characteristics of the dike crossing pipeline; finally, the pipeline coupled vibration characteristics are analyzed using the cross wavelet transform (CWT). The research results show that: 1) The vibration of the 6# dike crossing pipeline of Yang'er water plant is mainly caused by the multiple rotational frequency such as 29.5 Hz, 36.5 Hz and the leaf frequency 59.0 Hz; 2) The EWT method can effectively remove the interference signal and extract the characteristic frequencies 29.5 Hz, 36.5 Hz and 59.0 Hz; 3) Analyzing the coupled vibration characteristics of the dike crossing pipeline based on the CWT, the peak energy of the coupled vibration of the 6# pipeline is generally concentrated at the frequency of 29.5 Hz, and the source of the coupled vibration is the multiple rotational frequency of the 6# pipeline unit. The results of this study can offer new insights into the identification of vibration characteristics of the dike crossing pipeline, and can provide technical support for the analysis of vibration characteristics and reduction needs of similar projects.

1. Introduction

As an important part of the flood and tide control system of rivers, lakes, and seas, dike engineering is an important infrastructure to protect national economic construction and plays a very important role in national economic development as well as social harmony and stability [1]. With the rising demand for water in industry, agriculture, and other fields, the number of water supply pipelines has surged, and the structure of water supply networks has become increasingly complex. Pipeline crossing technology, characterized by

* Corresponding author. School of Water Resources, North China University of Water Resources and Electric Power, Zhengzhou, 450046, China.
E-mail addresses: 1657826640@qq.com (J. Huang), 201602416@stu.ncwu.edu.cn (Z. Li), zjwcivil@126.com (J. Zhang).
[1] Jinlin Huang and Ziyu Li have contributed equally to this work and should be considered co-first authors.

https://doi.org/10.1016/j.heliyon.2024.e37411
Received 26 April 2024; Received in revised form 29 August 2024; Accepted 3 September 2024
Available online 4 September 2024

minimal impact on traffic and natural waters, preservation of the natural environment, short construction cycles, and relatively low costs, has gained widespread use in urban water supply and conveyance engineering [2,3]. Most dike crossing pipelines are flow pressure pipelines, and under the influence of dynamic and control systems, water hammer frequently occurs, causing severe vibration and potentially leading to loosening and damage of pipeline joints. In recent years, scholars have conducted extensive research on the vibration characteristics of pipelines, yielding substantial findings.

In the analysis of pipeline structural characteristics, Liu [4] identifies the vibration characteristics of the circular tube by using the panoramic amplitude electronic speckle pattern interferometry and determines that the natural mode frequency of the structure would be significantly reduced by the axial crack; Liu [5] uses the wave propagation method to judge the dynamic characteristics of the buried pipeline filled with liquid, and finds that the natural vibration frequency of the pipeline is related to the type of media around the pipeline, which provides a new angle for the analysis of similar projects. In the study of fluid-structure interaction (FSI) characteristics of flow pipelines, Guo [6] puts forward an improved transfer matrix model to study the vibration characteristics of fluid conveying tube (FCP), it overcomes the disadvantage that the traditional transfer matrix model (TMM) can only be used to analyze the frequency response of FCP under point or pulsating excitation, the effects of the base amplitude, flow velocity and pressure on the vibration characteristics of parallel fluid conveying pipes (PFCP) are further studied; Quan [7] explores the axial vibration response characteristics of FSI vibration of hydraulic pipes, and verifies the correctness of the friction model through experiments, it is proved that the analytical accuracy of the axial velocity response of FSI vibration can be improved by considering the friction coupling. In the study of pipeline vibration characteristics under special loads, Jiang [8] summarizes the characteristics of buried pipeline under blasting vibration and vibration propagation characteristics, introduces the internal law of pipeline blasting vibration load, and comprehensively analyzes the dynamic failure mode and safety criterion of buried pipeline; Zhang [9] establishes the pipe-soil coupling vibration model for natural gas pipeline, and analyzes the relationship between pigging velocity and pipeline vibration through the finite element model. In pipeline vibration damping and control, Ding [10] proposes that a quasi-zero stiffness system composed of three linear springs be used as a nonlinear isolator to attenuate the lateral vibration of a fluid conveying pipeline caused by foundation excitation, it is found that the quasi-zero stiffness isolator can transfer several natural frequencies of pipe vibration to the low frequency region, and realize the high frequency region effective vibration isolation.

The above scholars have conducted research on the complex vibration characteristics of pipelines from the perspectives of numerical simulation, theoretical analysis, and model experiments, achieving excellent results. However, there are still some deficiencies in the study of the main vibration sources and their characteristics. The study of the cause and state of pipeline vibration based on prototype observation data is crucial for ensuring the safe and stable operation of pipelines. In hydraulic engineering practice, due to environmental disturbances affecting the collecting equipment and the complexity of the signals, a time-frequency analysis method is needed for comprehensive analysis.

Short-time Fourier transform (STFT) is an effective method for time-frequency analysis of non-stationary signals [11,12]. Chen [13] uses the STFT to identify the flow characteristics of multiphase flow in a pipeline. Jeon [14] proposes an area-efficient STFT processor for real-time and frequency analysis of non-stationary signals. Bykerk [15] proposes to use semi-permanent vibration acoustic sensors for leakage monitoring, and convolutional neural network (CNN) is trained based on the STFT of the acquired signals to achieve classification results for different operating and leakage situations. Although the STFT algorithm can do time-frequency analysis effectively, it still needs to set parameters artificially, and the analysis ability of abrupt signals is insufficient. Morlet put forward the concept of wavelet transform in 1974, and it has become an important method in the field of time-frequency analysis after continuous improvement [16,17]. Wang [18] uses continuous wavelet transform to extract different time-frequency components of electrocardiogram (ECG) signal, so as to achieve rapid identification of arrhythmia. Liu [19] uses wavelet transform to extract the characteristics of non-stationary wind power time series and uses the Long Short-Term Memory (LSTM) method to achieve short-term prediction of wind power. Perna [20] uses wavelet transform to analyze the fluid pressure signal of a pulsating heat pipe under different heat power input and realizes the visualization analysis of the main frequency of the pulsating heat pipe. Wavelet transform can overcome the problem of STFT parameter selection, effectively identify the time and frequency features of signal mutation, and realize the feature extraction in the time-frequency domain.

On the basis of the wavelet transform, in order to further analyze the correlation time-frequency characteristics between non-stationary signals, the cross wavelet transform (CWT) method is proposed [21]. Pagliaroli [22] analyzes the strong interaction relationship between the structure and the liquid in a hydraulic cantilever using the CWT; Ellis [23] analyzes the correlation between wind field short-time series and salinization response series, and identifies the relationship between wind-sand time and interval with the help of CWT; Dhar [24] realizes the effective classification and recognition of abnormal ECG signals by CWT and AlexNet CNN. Up to now, the CWT has become an important method in the field of signal correlation time-frequency characteristics analysis [25].

Under the excitation of overflow environments, the vibration characteristics of dike crossing pipelines are easily masked by noise and interference signals. Therefore, an effective signal processing method is required to extract the feature information of the pipeline vibration signal. Empirical mode decomposition (EMD) is an adaptive signal analysis method for dealing with non-linear and non-stationary signals [26,27]. Barbosh [28] gives a detailed description of the application of EMD methods in complex vibration signal processing and modal identification of civil structures. However, the decomposition process of EMD may cause boundary effects and mode mixing due to deficiencies in the computational theory of the algorithm [29,30]. In an attempt to decrease the interference of mode mixing, the ensemble empirical mode decomposition (EEMD) method is proposed [31,32]. Zhang [33] uses EEMD to process the vibration response signal of the overflow factory building and identify the vibration mode parameters of the structure. Gao [34] achieves early prediction of bearing faults by extracting weak fault signals from bearing vibration signals using the EEMD method. However, the effectiveness of the EEMD decomposition depends on the integration time and the amplitude of the added white noise [35], and mode mixing will not be mitigated if the parameters are not properly chosen. With the purpose of overcoming the above

problems, Gilles [36] proposes empirical wavelet transform (EWT), which combines the ideas of EMD and wavelet transform, has higher arithmetic precision and accuracy than EMD decomposition, and is able to adaptively decompose the signal and extract features. Peng [37] uses EWT to decompose the original energy consumption series, identifies the trend component and the cycle component of the original energy consumption data, and achieves high-precision prediction of energy consumption with the LSTM method. Liu [38] uses the EWT algorithm to suppress the noise to the modal interference, extracts time-domain, frequency-domain, amplitude-domain features and obtains bearing structure fault information. Yu [39] uses EWT to decompose the three-channel vibration signals of hydraulic pumps, and fuses the decomposed signals using variance contribution rate to realize the frequency identification of weak fault characteristics of hydraulic pumps.

In summary, CWT is an effective method for time-frequency characteristic analysis of related sequences, and EWT is effective for data noise removal and feature extraction. To address the challenge of effectively identifying the vibration characteristics of dike crossing pipelines, this paper proposes a method for analyzing vibration characteristics based on EWT and CWT. Firstly, the effectiveness of wavelet transform, EWT and CWT in signal processing is verified with the help of simulation signal analysis; Then, taking the 6# dike crossing pipeline of Yang'er water plant in Foshan city, Guangdong province as the research object, based on the prototype observation data, the mutual correlation power spectrum is used to identify the main sources of vibration and the EWT method is used to extract the characteristics of the pipeline's main vibration sources; Finally, the wavelet transform method is applied to identify the influence of the vibration sources in the time domain, and the cross wavelet transform is applied to identify the coupled vibration characteristics of the dike crossing pipeline. This study provides a theoretical basis for identifying vibration characteristics, offers technical support for pipeline vibration reduction, and ensures the safe operation of dike crossing pipelines.

2. Methodology

2.1. Wavelet transform algorithm

Wavelet transform can effectively identify the time-frequency characteristics of a signal by stretching or compressing the wavelet basis function to make the wavelet basis function converge to the original signal [16,40]. For the energy limited signal $x(t)$, there is the following equation:

$$x(t) \in L^2(R) \Leftrightarrow \int_R |x(t)|^2 dt < +\infty \tag{1}$$

The wavelet transform integrates the function clusters $\psi_{a,\tau}(t)$ and $x(t)$ as follows:

$$WT_x(a,\tau) = \frac{1}{\sqrt{a}} \int_{-\infty}^{+\infty} x(t)\psi_{a,\tau}(t)\mathrm{d}t, \quad a > 0 \tag{2}$$

where: $WT_x(a,\tau)$ is the wavelet transform, τ is the time factor, and a is the scale factor.

The function cluster $\psi_{a,\tau}(t)$ consists of the wavelet basis functions $\psi(t)$ and behaves as follows:

$$\psi_{a,\tau}(t) = \frac{1}{\sqrt{a}} \psi\left(\frac{t-\tau}{a}\right) (a > 0, \tau \in R) \tag{3}$$

that is

$$\psi_{a,\tau}(t)^2 = \int_{-\infty}^{+\infty} |\psi_{a,\tau}(t)|^2 \mathrm{d}t = \int_{-\infty}^{+\infty} |\psi(t)| \mathrm{d}t \tag{4}$$

From Eq. (4), it can be seen that the essence of wavelet transform is to converge stretchable cluster functions to the signal $x(t)$. Through the process of wavelet transform, the signal $x(t)$ time and frequency characteristics are identified.

2.2. Empirical wavelet transform

2.2.1. Empirical mode decomposition

Empirical mode decomposition (EMD) is proposed by Huang [26], this method adaptively decomposes the signal into characteristic intrinsic mode function (IMF), which is widely used in the field of vibration signal analysis.

The computational procedure is as follows: between the maximum and minimum values of a set of original signals $x(t)$, the mean value $m_1(t)$ is obtained by interpolation of the spline function with the upper and lower envelopes fitted. $x(t)$ minus $m_1(t)$ to get the signal value $h_1(t)$:

$$h_1(t) = x(t) - m_1(t) \tag{5}$$

If $h_1(t)$ can satisfy the two conditions of the IMF component and the sieve termination criterion, then $h_1(t)$ is the first IMF. If $h_1(t)$ cannot satisfy the characteristics of the IMF component, $h_1(t)$ is treated as the original signal and the computation is continued until the data $h_{1k}(t)$ is obtained for the k-th time that satisfies the characteristics of the IMF:

$$h_{1k}(t) = h_{1(k-1)}(t) - m_{1k}(t) \tag{6}$$

Let the first order IMF component be $c_1(t)$, $x(t)$ minus $c_1(t)$ to obtain the residual $r_1(t)$.

$$r_1(t) = x(t) - c_1(t) \tag{7}$$

Using $r_1(t)$ as a new signal, the above steps are repeated until the second IMF is obtained that satisfies the requirement. Multiple IMFs are obtained by cyclically calculating according to the above steps. The decomposition terminates when the residual is a monotonic function. The signal $x(t)$ can be expressed as

$$x(t) = \sum_{i=1}^{n} c_i(t) + r_n(t) \tag{8}$$

2.2.2. Empirical wavelet transform

EMD is computationally intensive and prone to mode confusion, causing the loss of effective feature information in the original signal. Building on previous results, Gilles combined wavelet transform theory with the EMD method to propose the EWT method. EWT provides theoretical robustness, complete adaptivity, swift computational capabilities, and effectively circumvents mode mixing issues [36]. The EWT performs spectrum banding based on the Fourier transform of the signal to obtain the closely connected amplitude modulation-frequency modulation (AM-FM) functions with the help of a band-pass filter bank. Based on this, the adaptive decomposition of the signal is achieved and the intrinsic mode function (IMF) of the vibration signal is obtained.

The proper division of the Fourier spectrum of the vibration signal by using the EWT algorithm is the basis of signal adaptive analysis. In the signal spectrum, the appropriate number of segments N and boundaries ω_n are important factors that determine whether the signal features can be divided effectively. Taking Fourier support $[0, \pi]$ as an example, when two known boundaries of 0 and π are removed, there are still $N-1$ boundaries to be determined. During the Fourier spectrum decomposition, $[0, \pi]$ is divided into N segments, ω_n is used to represent the boundary of each segment ($\omega_0 = 0$, $\omega_N = \pi$), the segmented spectrum is defined as $\Lambda_n = [\omega_{n-1}, \omega_n]$, and for each ω_n, the transition region of $T_n = 2\tau_n$ is defined. The decomposition process is shown in Fig. 1.

When $n > 0$, the empirical scale function $\phi_n(\omega)$ and the empirical wavelet function $\psi_n(\omega)$ can be defined as:

$$\phi_n(\omega) = \begin{cases} 1 & |\omega| \le (1-\gamma)\omega_m \\ \cos\left[\frac{\pi}{2}\beta\left(\frac{1}{2\gamma\omega_n}(|\omega| - (1-\gamma)\omega_m)\right)\right] & (1-\gamma)\omega_{n+1} \le |\omega| \le (1+\gamma)\omega_{n+1} \\ 0 & otherwise \end{cases} \tag{9}$$

$$\psi_n(\omega) = \begin{cases} 1 & (1+\gamma)\omega_n \le |\omega| \le (1-\gamma)\omega_{n+1} \\ \cos\left[\frac{\pi}{2}\beta\left(\frac{1}{2\gamma\omega_{n+1}}(|\omega| - (1-\gamma)\omega_{n+1})\right)\right] & (1-\gamma)\omega_{n+1} \le |\omega| \le (1+\gamma)\omega_{n+1} \\ \sin\left[\frac{\pi}{2}\beta\left(\frac{1}{2\gamma\omega_n}(|\omega| - (1-\gamma)\omega_n)\right)\right] & (1-\gamma)\omega_n \le |\omega| \le (1+\gamma)\omega_n \\ 0 & otherwise \end{cases} \tag{10}$$

where: $\tau_n = \gamma\omega_n, 0 < \gamma < 1$, $\gamma = \min_n\left(\frac{\omega_{n+1}-\omega_n}{\omega_{n+1}+\omega_n}\right)$, $\beta(x) = x^4(35 - 84x + 70x^2 - 20x^3)$, $x \in [0,1]$.

The detail function of EWT is $W_f^e(n,t)$ and the approximate function is $W_f^e(0,t)$. The inner product of the empirical wavelet function $\psi_n(\omega)$ and the empirical scale function $\phi_1(\omega)$ with the signal $f(t)$, respectively, leads to the following equation:

$$W_f^e(i,t) = \langle f(t), \psi_i(t)\rangle = F^{-1}[f(\omega)\psi_i(\omega)] \tag{11}$$

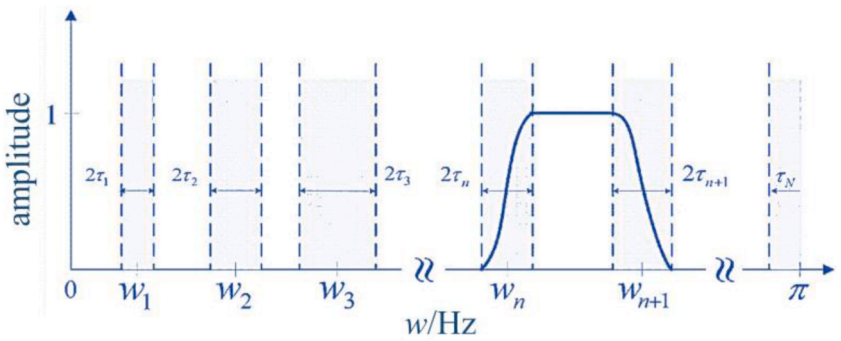

Fig. 1. The division of the Fourier spectrum.

$$W_f^e(0,t) = \langle f(t), \phi_1(t) \rangle = F^{-1}[f(\omega)\phi_1(\omega)] \tag{12}$$

where: $F^{-1}[\cdot]$ is the inverse Fourier transform, $i = 1, 2, \ldots N$.

The reconstructed signal $f(t)$ is

$$\begin{aligned} f(t) &= W_f^e(0,t) \otimes \phi_1(t) + \sum_{n-1}^{N} W_f^e(i,t) \otimes \psi_i(t) \\ &= F^{-1}\left[\widehat{W}_f^e(0,\omega) \otimes \phi_1(\omega) + \sum_{n-1}^{N} \widehat{W}_f^e(i,\omega) \otimes \psi_i(\omega) \right] \end{aligned} \tag{13}$$

where: $\otimes$ stands for convolution; $\widehat{W}_f^e(0,\omega)$ and $\widehat{W}_f^e(i,\omega)$ represent the Fourier transform of $W_f^e(0,t)$ and $W_f^e(i,t)$.

Mode function $f_k(t)$ is defined as follows:

$$f_0(t) = W_f^e(0,t) \otimes \phi_1(t) \tag{14}$$

$$f_k(t) = W_f^e(k,t) \otimes \phi_k(t) \tag{15}$$

where: $k = 1, 2 \ldots N-1$.

2.2.3. The optimal decomposition order N

Before the EWT of the signal, an optimization strategy for mode parameter identification is proposed to reduce the subjective error caused by artificially setting the EWT decomposition parameter N. According to the EWT decomposition equation, the total energy of the original signal is the sum of the energies of each component. During decomposition, energy leakage can cause the sum of the component energies to be less than the total energy of the original signal. However, if the decomposition order N is set too high, virtual components may appear, increasing the total energy of the components. Based on this theory, Eq. (16) is established to distinguish the optimal decomposition order.

$$\begin{cases} E_N^l = \sqrt{\dfrac{\sum_{i=1}^{n} x_l^2(i)}{n}}, l = 1, 2, \cdots N \\ E_N = \sum_{l=1}^{N} E_N^l \\ \theta_{N,N-1} = \dfrac{|E_N - E_{N-1}|}{E_{N-1}} \end{cases} \tag{16}$$

where: E_N^l is the energy of each component signal, E_N is the sum of the energy of the N components obtained by decomposition, and $\theta_{N,N-1}$ represents the energy difference of the component signal under different N values.

The optimal N value is determined by calculating the $\theta_{N,N-1}$ for the component signals and analyzing the change in $\theta_{N,N-1}$ for different N values. When $\theta_{N,N-1}$ becomes small, it means that the signal is decomposed normally; when $\theta_{N,N-1}$ suddenly becomes larger, it shows that the EWT decomposition process appears the phenomenon of over-decomposition, resulting in false components. At this time, the corresponding decomposition times $N-1$ is the optimal decomposition order of EWT.

In summary, the main process of EWT is shown in Fig. 2.

2.3. Cross wavelet transform

In order to further analyze the common time-frequency characteristics between the correlated signals, we propose the cross wavelet transform algorithm based on the wavelet transform algorithm. For an energy limited signal $x(t)$, there is wavelet transform as:

$$WT_x(a,\tau) = \frac{1}{\sqrt{a}} \int_{-\infty}^{+\infty} x(t) \psi_{a,\tau}(t) \mathrm{d}t, a > 0 \tag{17}$$

For signal $y(t)$, there is $WT_y(a,\tau)$, let the cross wavelet transform of $x(t)$ and $y(t)$ be [41]:

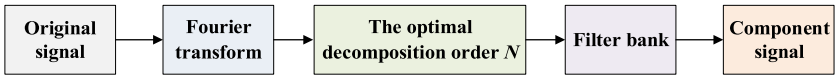

Fig. 2. The process of the EWT method.

$$CWT(a,\tau) = WT_x(a,\tau)WT_y^*(a,\tau) \tag{18}$$

The cross wavelet scale spectrum (CWS) is:

$$CWS(a,\tau) = CWT(a,\tau)CWT^*(a,\tau) = |CWT(a,\tau)|^2 \tag{19}$$

Leveraging cross wavelet transform, this study simultaneously analyzes the time and frequency domain characteristics of signals, extracts common features between correlated signals, and investigates the correlation and related features among vibration signals, thereby broadening the scope of vibration signal analysis.

3. Simulation analysis

Simulation signals with the same frequency characteristics but different time domain distributions are constructed and simulation tests are carried out to analyze each method. The simulation signals are as follows:

$$s1 = \begin{cases} \sin(6\pi t) & 0 \le t < 2\text{s}, 4 < t \le 6\text{s} \\ \sin(6\pi t) + \sin(14\pi t) & 2 \le t \le 4\text{s} \end{cases} \tag{20}$$

$$s2 = \begin{cases} \sin(6\pi t) & 0 \le t < 4\text{s} \\ \sin(6\pi t) + \sin(14\pi t) & 4 \le t \le 6\text{s} \end{cases} \tag{21}$$

Set the sampling frequency to 100 Hz, for the signals $s1$ and $s2$, with the help of Fourier transform, the respective signal time course diagrams and power spectrum density diagrams can be obtained as Fig. 3(a–d).

By comparing the time course of the signals $s1$ and $s2$, it can be seen that although both signals have the same components, each component occupies different period, and the moments of the peaks are also different. Comparing the power spectrum density from the Fourier transform of the signals $s1$ and $s2$, the two signals have the same main frequency and main frequency energy, with the main frequencies of 3 Hz and 7 Hz, respectively, which is consistent with the frequency characteristics of the signal construction. Comparing and analyzing the time course diagrams and power spectrum density diagrams of $s1$ and $s2$, it can be seen that the Fourier transform has a high discriminative ability in frequency domain feature recognition, but it cannot accurately locate the moments corresponding to each signal frequency feature, which has some limitations in the analysis of vibration signals.

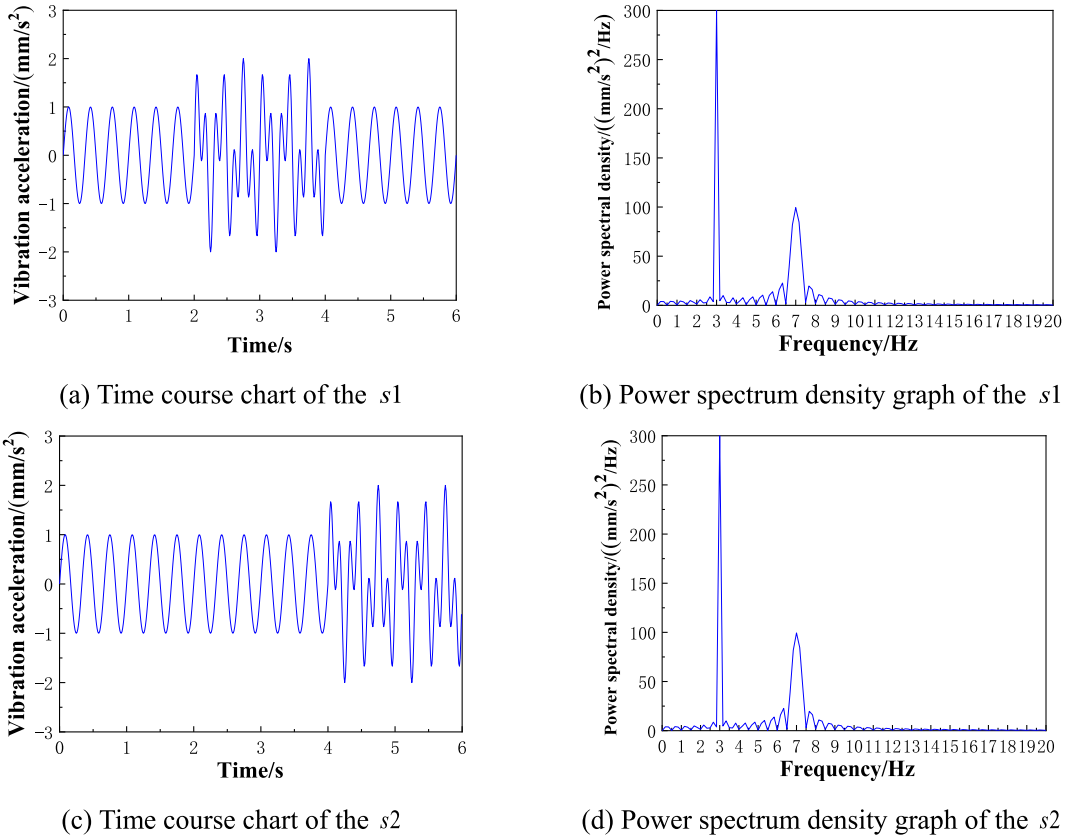

Fig. 3. Time-course and power spectrum density graph of the simulation signals $s1$ and $s2$.

3.1. Wavelet transform simulation analysis

The signals $s1$ and $s2$ are analyzed by wavelet transform and the results are shown in Fig. 4(a and b).

Fig. 4 clearly shows the wavelet transform results of the signals. The wavelet transform coefficients exhibit different peaks at various frequencies and times, indicating that the wavelet transform can simultaneously analyze both time-domain and frequency-domain characteristics of the signal. In the wavelet transform results of vibration signals, the x-axis represents time, the y-axis represents frequency, and the z-axis represents the amplitude of the wavelet transform coefficients. These elements complement each other, forming a three-dimensional map. However, in the three-dimensional image, the coordinate information cannot be read accurately, which affects the quality of analysis, so the three-dimensional image is simplified to a two-dimensional graph, the x-axis represents the time, the y-axis represents the frequency, and the amplitude of the transform coefficients of the corresponding points is indicated by the color, the amplitude from large to small corresponding to the color of the light to dark, which is easy to observe and study, and the time-wavelet scale spectrum of the signals $s1$ and $s2$ respectively are shown in Fig. 5(a and b).

Comparing Fig. 5(a) and (b), it can be seen that the main frequency characteristics are still 3 Hz and 7 Hz. 3 Hz frequency corresponds to the same distribution of amplitude energy in the time domain, and 7 Hz frequency mainly appears in the wavelet transform results of the signal $s1$ at the position of 2∼4s, and the vibration signal $s2$ mainly appears in the wavelet transform results of the vibration signal at the position of 4∼6s, which is basically the same as that in the composition of the signals in Eq. (20) and Eq. (21). Wavelet transform can accurately reflect the frequency distribution in the time domain and clearly identify the frequency characteristics of vibration signals. This method offers precise analysis results and strong adaptive capabilities, making it widely applicable in signal analysis.

3.2. Empirical wavelet transform simulation analysis

The EWT can adaptively decompose the frequency characteristics of vibration signals, effectively avoid over-decomposition and mode mixing, eliminat errors from artificial parameter settings, and achieve significant results in signal feature extraction and analysis.

The EWT is performed on the two simulation signals. The optimal decomposition order N is judged in Fig. 6.

From Fig. 6, $\theta_{N,N-1}$ increases rapidly when N is 3, indicating that a spurious component may be present, so $N = 2$ is taken as the optimal decomposition order. The results of the frequency domain division are shown in Fig. 7(a and b).

As can be seen from Fig. 7, the simulation signal of a multi-source combination can be decomposed into multiple component signals used by EWT. Since the simulation signals $s1$ and $s2$ have the same constituent elements, the Fourier spectrum of the two signals are same, and the frequency division results of the two signals are similar when the EWT is performed. In the following, the EWT decomposition results of the signals $s1$ and $s2$ are shown in Fig. 8(a - d) and Fig. 9(a–d), respectively.

From the EWT decomposition results, it can be seen that the EWT can be used to extract the two sources of the signal, 3 Hz and 7 Hz. Although the whole process is affected by the 3 Hz signal, the corresponding signal of 7 Hz can still be decomposed and the component signal with 7 Hz as the main frequency can be obtained. This shows that the EWT has good applicability and effectiveness in multi-source signal decomposition and analysis.

In the following, the time-domain distribution characteristics of the component signals are analyzed with the help of wavelet transform to check whether the EWT results coincide with the actual composition of the signals. Time-wavelet scale spectrum for the IMF are shown in Fig. 10(a–d).

As can be seen from Fig. 10(a–d), the IMF1 of the signal $s1$ and $s2$ characteristics have similar characteristics, corresponding to a

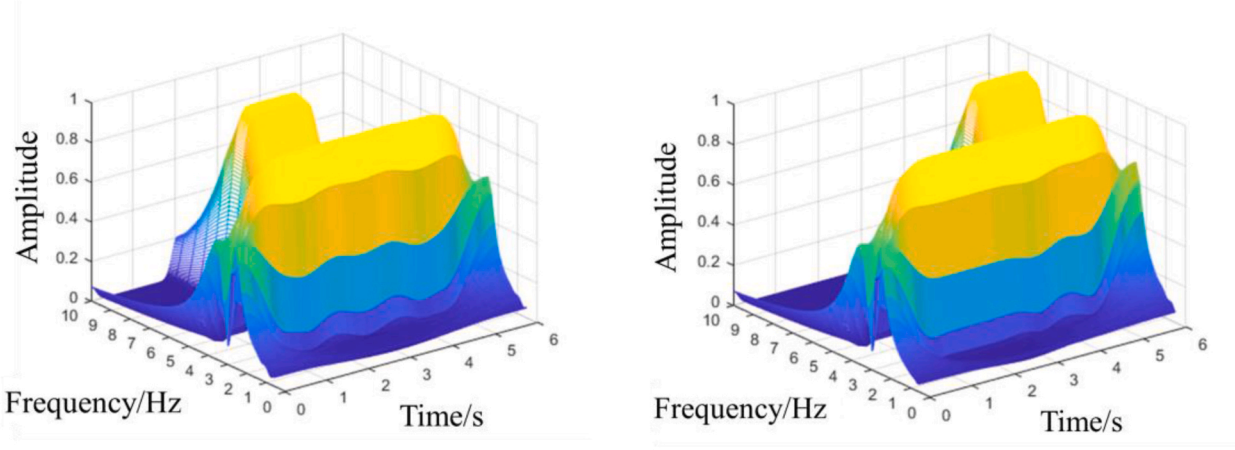

Fig. 4. Wavelet transform results of the signals $s1$ and $s2$.

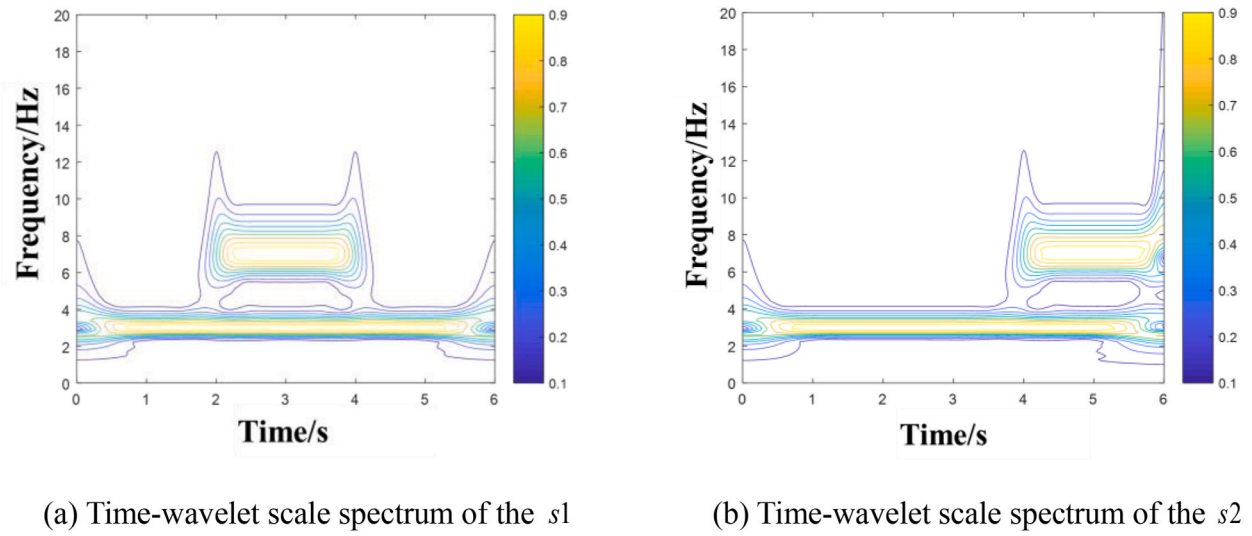

Fig. 5. Time-wavelet scale spectrum of the signals $s1$ and the $s2$.

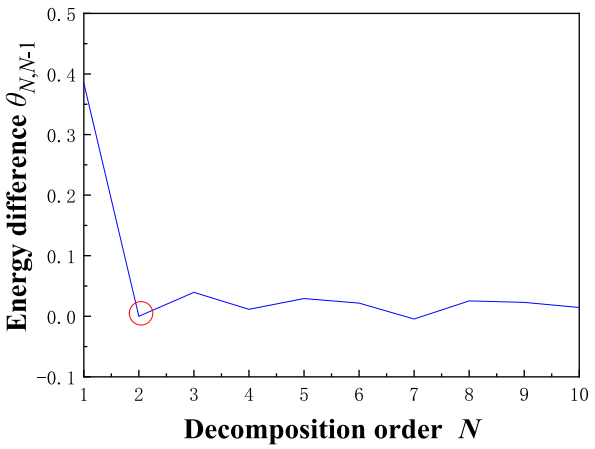

Fig. 6. Total energy difference curve of the $\theta_{N,N-1}$ of simulation signal.

major frequency of 3 Hz and a major time-domain energy distribution of 0–6 s. The IMF2 of the signal $s1$ and $s2$ corresponds to a major frequency of 7 Hz and the main time-domain energy distribution are 2∼4s and 4∼6s, respectively. This demonstrates that the EWT can extract IMFs consistent with the signal's characteristics in both time and frequency domains, providing favorable conditions for subsequent signal analysis.

3.3. Cross wavelet transform simulation analysis

For vibration signal analysis, the cross wavelet transform can effectively identify the main features of the signal and accurately extract the correlation feature between two signals. The cross wavelet transform is performed on the simulation signals $s1$ and $s2$, and the cross time-wavelet scale spectrum is obtained, as shown in Fig. 11.

From the cross time-wavelet scale spectrum, it can be seen that the main correlation frequency of the two signals is 3 Hz, which exists in the whole time course of the two signals. In addition, at 4s, the peak energy of the correlation frequency of both signals corresponds to 7 Hz, indicating that the frequency 7 Hz appears in both signals at the moment of 4s. It can be seen that the cross wavelet transform can not only clearly identify the stable correlation frequency of 3 Hz and the change correlation frequency of 7 Hz between two signals, but also accurately determine the moment when the 7 Hz frequency occurs in two signals at the same time. The method has the advantages of high sensitivity and accuracy in analyzing the time-frequency domain characteristics of correlated signals.

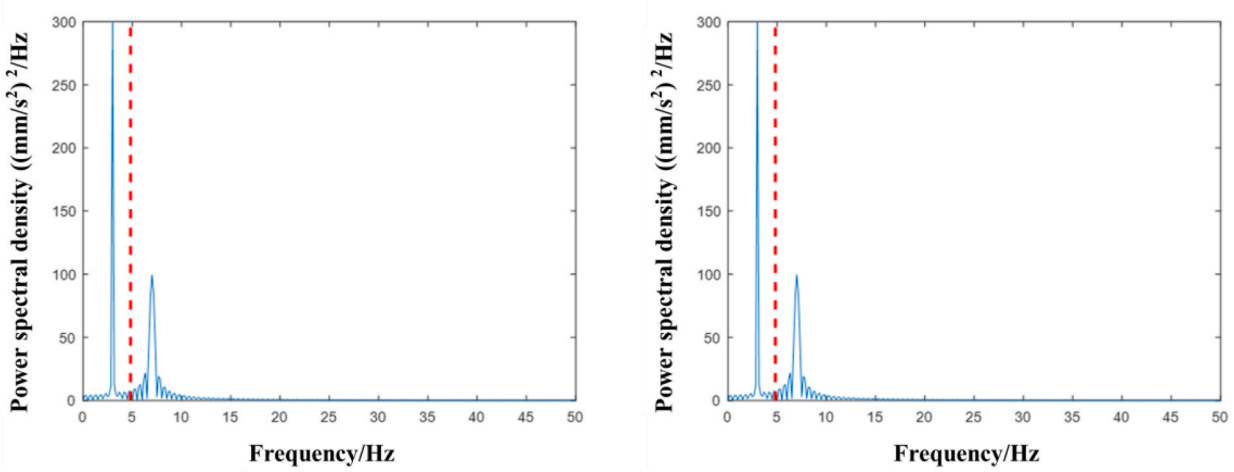

(a) Frequency domain division result of $s1$ (b) Frequency domain division result of $s2$

Fig. 7. Frequency domain division result of the $s1$ and $s2$.

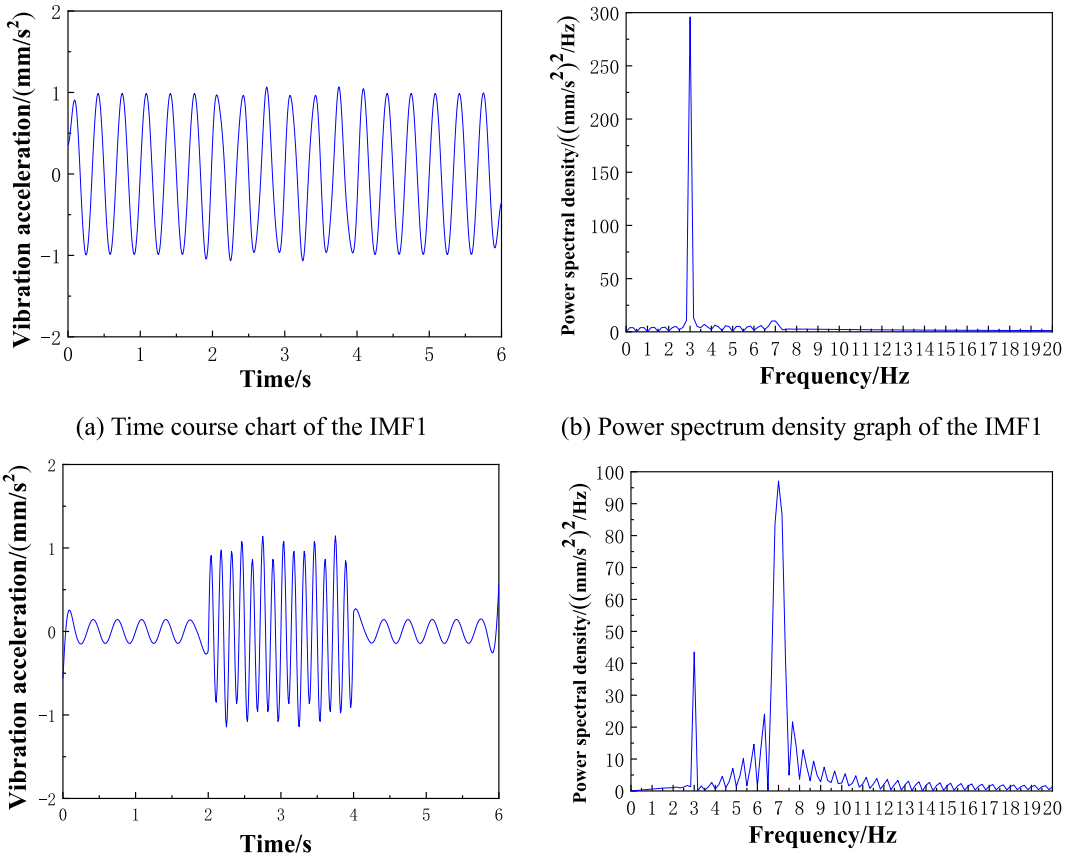

(a) Time course chart of the IMF1 (b) Power spectrum density graph of the IMF1

(c) Time course chart of the IMF2 (d) Power spectrum density graph of the IMF2

Fig. 8. EWT decomposition results of simulation signal $s1$.

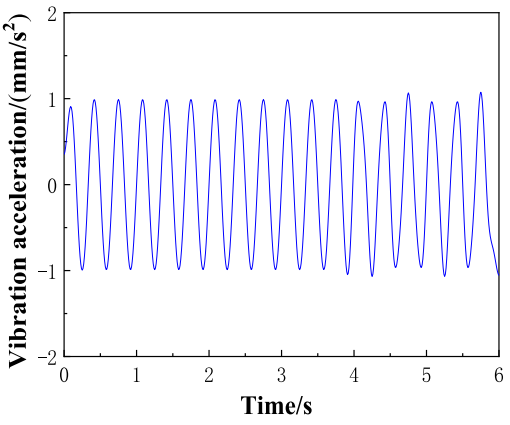

(a) Time course chart of the IMF1

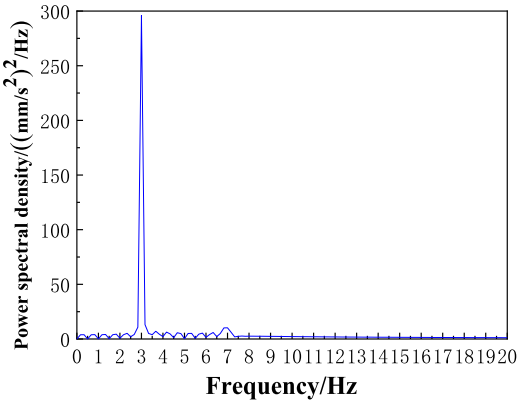

(b) Power spectrum density graph of the IMF1

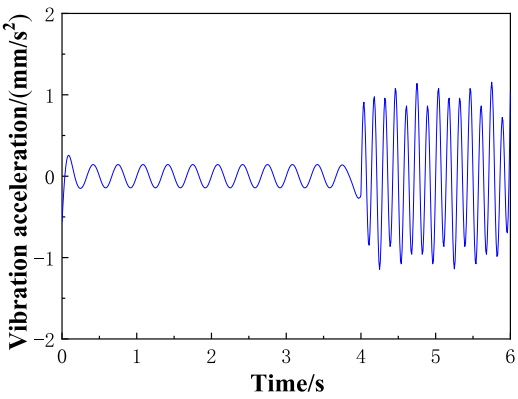

(c) Time course chart of the IMF2

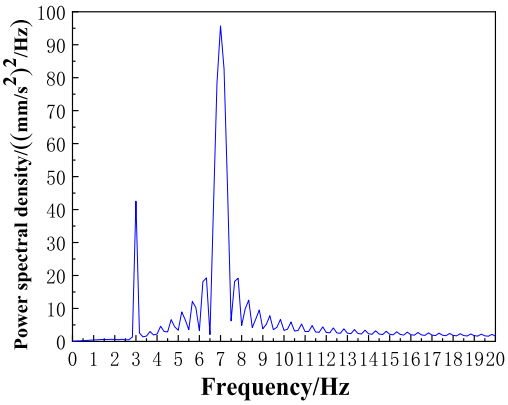

(d) Power spectrum density graph of the IMF2

Fig. 9. EWT decomposition results of simulation signal *s*2.

4. Engineering example

4.1. Project summary

Yang'er water plant is located in Shunde district, Foshan city, Guangdong province. The water plant is adjacent to the dike of the Shunde waterway, which was constructed in 1992 and reconstructed in 1997 with a production scale of 12101 × 10^4 m^3/a water and a plant area of 90440 m^2. At present, Yang'er water plant is a high quality drinking water source in Shunde, with a daily water supply capacity of 400,000 m^3, which provides important support for the development of the regional industry and brings significant social and economic benefits. Fig. 12(a, b) is the dike crossing pipe of Yang'er water plant.

There are nine DN600 water supply pipelines set up in Yang'er water plant, and the pumps are MOTOR M43-44-8AA/01 (rated speed 730 r/min) and MOTOR M54-38-10AA/01 (rated speed 590 r/min) with a single machine flow rate of 3 m^3/s. The main object of study in this paper is the 6# dike crossing pipeline.

Four measurement points are arranged, measurement point 1 is arranged at the inlet bend of the pipeline in the pump house, measurement point 2 is arranged in the straight section after the pipeline exits the pump house, measurement point 3 is arranged on the pier where the pipeline enter the dike, and measurement point 4 is arranged in the straight section after the pipeline exit the dike, as shown in Figs. 13 and 14.

This prototype observation uses the sensors for 891-2 low frequency pickup, which has a sensitivity of 0.1v*s/m, a measurement accuracy of 0.01 %, and a measurement range of 0.5–100Hz. By combining the 891-2 low frequency pickup with the data acquisition & signal processing (DASP) system, multiple channels of signals can be collected and stored to ensure the true and comprehensive collection of vibration acceleration signals from the dike crossing pipeline. In addition, three working conditions are set up and the description are shown in Table 1. In Table 1, the process of 6# Pipeline unit startup means that the unit speed reaches stability from 0 r/min, the process of the unit shutdown means that the speed decreases from stability to 0 r/min, and normal operation means that the unit speed is in a stable state.

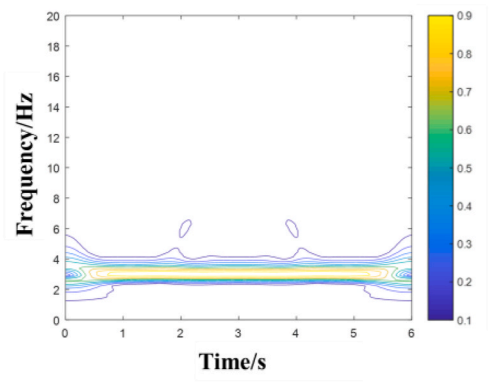

(a) Time-wavelet scale spectrum for the IMF1 of the $s1$

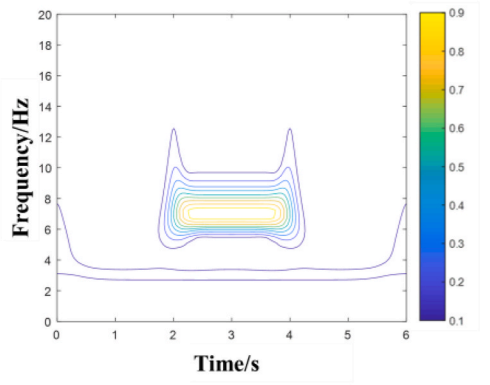

(b) Time-wavelet scale spectrum for the IMF2 of the $s1$

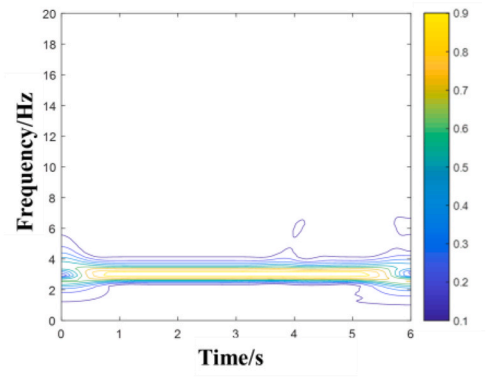

(c) Time-wavelet scale spectrum for the IMF1 of the $s2$

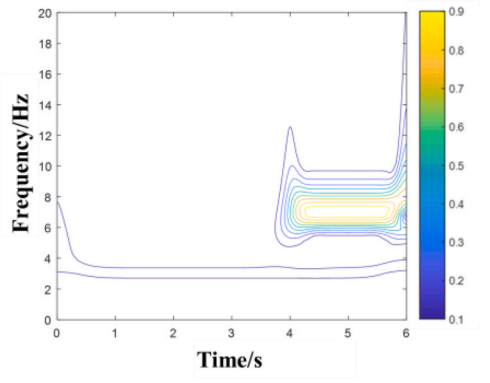

(d) Time-wavelet scale spectrum for the IMF2of the $s2$

Fig. 10. Time-wavelet scale spectrum for the IMF of the $s1$ and $s2$.

4.2. Main vibration source analysis of the dike crossing pipeline

The mutual correlation function reflects the mutual matching between two functions, and the Fourier transform of the mutual correlation function is called the mutual correlation power spectrum [42].

For the signals $f(x,y)$ and $g(x,y)$, there is a mutual correlation power spectrum:

$$W_{f,g}(u,v) = F(u,v)G^*(u,v) \tag{22}$$

Where: $F(u,v)$ is the Fourier transform of $f(x,y)$ and $G^*(u,v)$ is the complex conjugate of the Fourier transform of $g(x,y)$.

In order to obtain the main correlation frequency between the measurement points and derive the main source of vibration that causes the synchronous vibration of each measurement point, this section applies the Fourier transform based mutual correlation analysis method to obtain the mutual correlation power spectrum and achieve the analysis of the correlation frequency of the measurement points.

Firstly, the correlation frequency analysis is carried out by taking the X-direction measurement point of the shutdown condition as an example, and the result of the cross-correlation power spectrum is shown in Fig. 15(a–f).

Similarly, the cross-correlation power spectrum of the signals of the measurement points in the startup condition and the normal operation condition are analyzed. The number of occurrences of different peaks in the cross-correlation power spectrum of the measurement points under the three operating conditions is counted, and the results are shown in Fig. 16(a–c).

Comprehensively analyzing the above three statistical graphs, among the multiple correlation frequencies between different measurement points under the three working conditions, 29.5 Hz, 36.5 Hz and 59.0 Hz appeared the most, indicating that these three frequencies have a greater impact on the vibration of each measurement point, have a certain degree of correlation between the measurement points, and are the main factors leading to the vibration of the pipeline.

Analyzing whether the characteristic frequency obtained is correct according to the situation of the field equipment. The rated

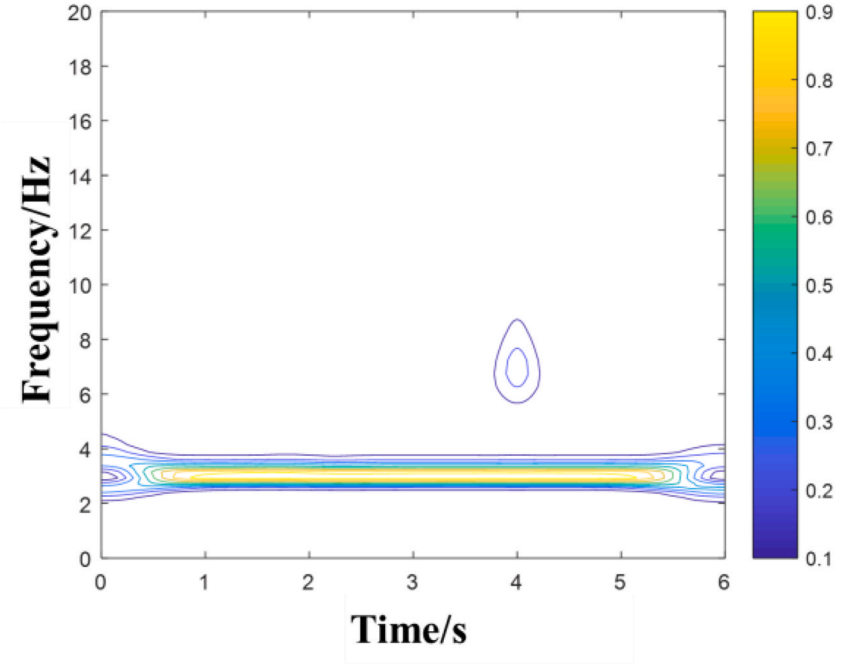

Fig. 11. Cross time-wavelet scale spectrum of the *s*1 and *s*2.

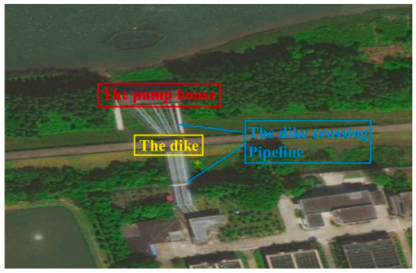

(a) Satellite view of the dike crossing pipeline at the Yang'er water plant

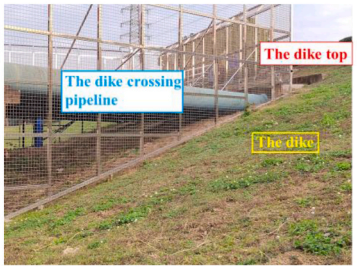

(b) Side view of the dike crossing pipeline

Fig. 12. The dike crossing pipeline of Yang'er water plant.

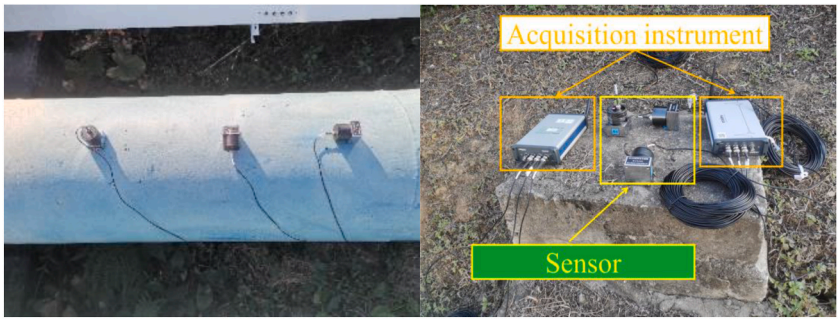

Fig. 13. Pickup arrangement.

speed of the unit of 6# pipeline is 590 r/min, and the rotational frequency is 9.83 Hz; the rated speed of the unit of 7# pipeline is 730 r/min, and the rotational frequency is 12.16 Hz. Because 29.5 Hz and 36.5 Hz are multiple times of 9.83 Hz and 12.16 Hz, the vibration source with main frequency of 29.5 Hz and 36.5 Hz is the multiple rotational frequency; 6# pipeline unit rotational frequency is 9.83

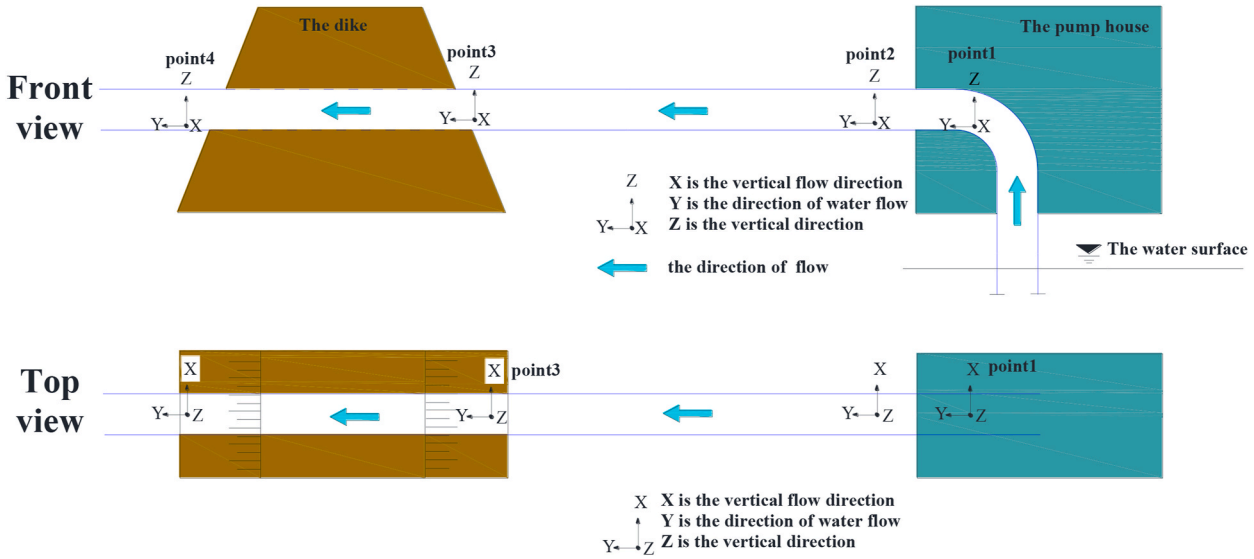

Fig. 14. Measurement point arrangement.

Table 1
Conditions for testing a prototype pipeline.

working condition	Description of working conditions	Sampling time/s	Frequency/Hz	Sensors	Signal type
1	6# Pipeline unit shutdown	100	512	891–2	acceleration
2	6# Pipeline unit startup	100	512	891–2	acceleration
3	6# Pipeline unit normal operation	100	512	891–2	acceleration

Hz, the pump has six sets of blades, corresponding to the unit leaf frequency is 59.0 Hz, the vibration source with main frequency of 59.0 Hz is the unit leaf frequency.

Since the cross-correlation power spectrum is based on Fourier transform, it is not possible to get the time characteristics of the frequency with correlation, and the distribution of the cross-correlation power spectrum is same in each direction under each working condition, it is difficult to obtain the influence of different vibration sources on the vibration of the measuring point.

Therefore, the three main correlation frequencies of 29.5 Hz, 36.5 Hz, and 59.0 Hz are the focus of subsequent analysis, aiming to clarify the influence of main vibration sources on the pipeline's vibration process using wavelet transform and cross wavelet transform.

4.3. Feature information extraction of the dike crossing pipeline

On the basis of clarifying 29.5 Hz, 36.5 Hz and 59.0 Hz as the main characteristic frequencies, feature information extraction is carried out on the signals with the help of the EWT method. Take the vibration signal collected in the Y-direction at measurement point 1 under the shutdown condition of the 6# pipeline as an example to show the process of feature information extraction. The vibration time course diagram and power spectrum density diagram of the signal are shown in Fig. 17(a and b). It can be seen that there are many interference signals with unknown frequency and high-frequency noise in the original signal, which can't get the real feature information of the vibration signal directly.

According to Eq. (16) to determine the best decomposition order N of EWT for the signal, the calculation results of $\theta_{N,N-1}$ are shown in Fig. 18.

According to Fig. 18, it can be found that $\theta_{N,N-1}$ increases rapidly when $N = 7$. When $N = 6$, $\theta_{N,N-1}$ increases by 0.005 and when $N = 7$, $\theta_{N,N-1}$ suddenly increases by 0.06, suggesting that a false component may be present. So $N = 6$ is taken as the best decomposition order, and the Fourier spectrum of this signal is divided by using EWT algorithm. The result is shown in Fig. 19.

By EWT decomposition, the signal is decomposed into six feature components, the time course diagram and power spectrum density diagram of each feature component are shown in Fig. 20(a–l).

According to the EWT decomposition results, IMF1 shows low-frequency vibration of the pipeline caused by the water flow factor, which corresponds to a low amplitude; IMF2~IMF3 show high-frequency vibration with the main frequency of 29.5 Hz and 36.5 Hz; IMF4~IMF5 show a cluster of signals without a clear main frequency centered on 40 Hz and 50 Hz; IMF6 shows high-frequency vibration with a main frequency of 59.0 Hz and mixed with a large amount of noise. Because IMF4~IMF5 features are blurred with low energy values, they are considered as interference signals. The IMF4~IMF5 should be removed, IMF1~IMF3 and IMF6 should be retained. Singular value decomposition (SVD) is a traditional and effective method of noise removal [43]. The interference noise

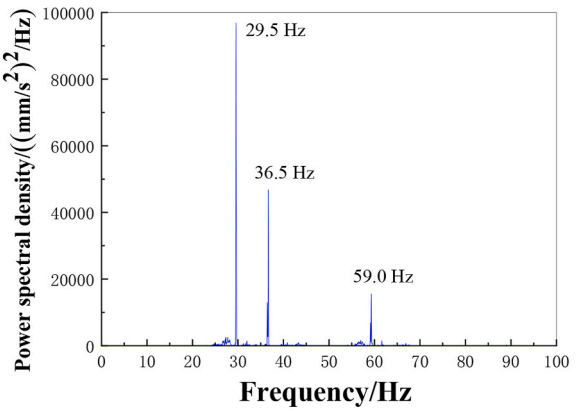

(a) Cross-correlation power spectrum of measurement point 1 and measurement point 2

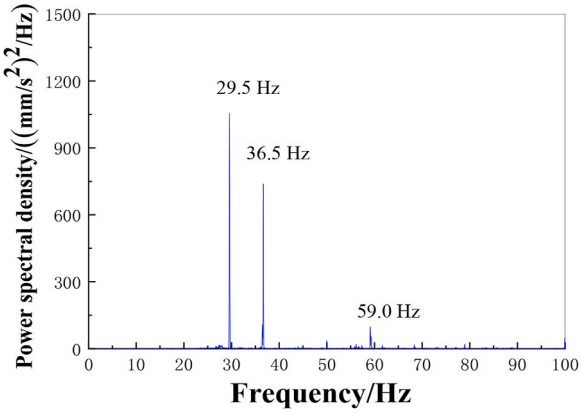

(b) Cross-correlation power spectrum of measurement point 1 and measurement point 3

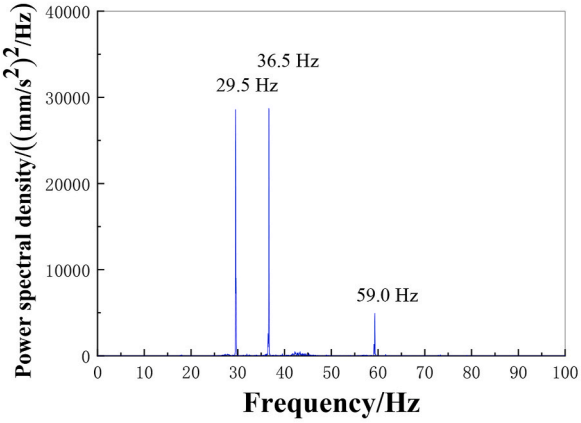

(c) Cross-correlation power spectrum of measurement point 1 and measurement point 4

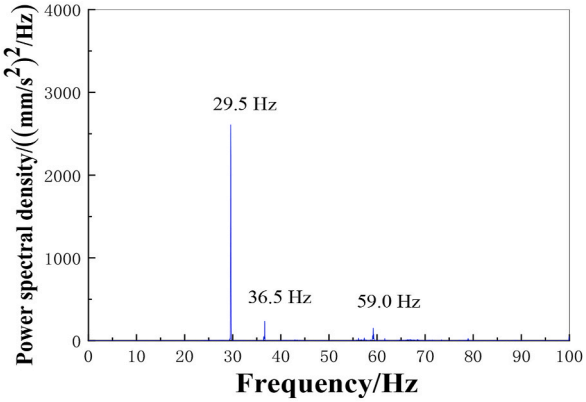

(d) Cross-correlation power spectrum of measurement point 2 and measurement point 3

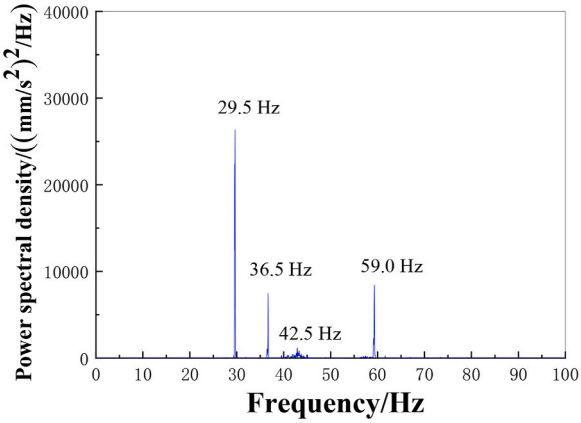

(e) Cross-correlation power spectrum of measurement point 2 and measurement point 4

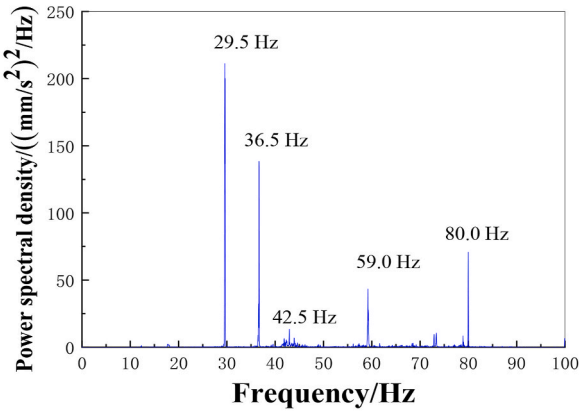

(f) Cross-correlation power spectrum of measurement point 3 and measurement point 4

Fig. 15. Cross-correlation power spectrum of X-direction measurement signals under shutdown conditions.

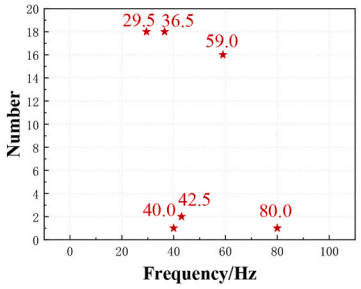

(a) Statistical plot of the number of peak in cross-correlation power spectrum under the shutdown condition

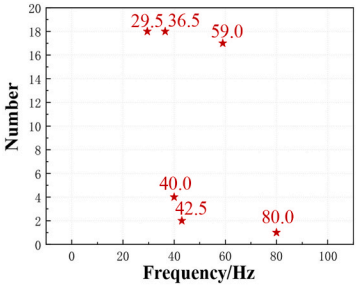

(b) Statistical plot of the number of peak in cross-correlation power spectrum under the startup condition

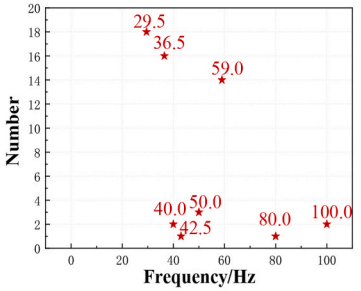

(c) Statistical plot of the number of peak in cross-correlation power spectrum under the normal operation condition

Fig. 16. Statistical plot of the number of peak in cross-correlation power spectrum.

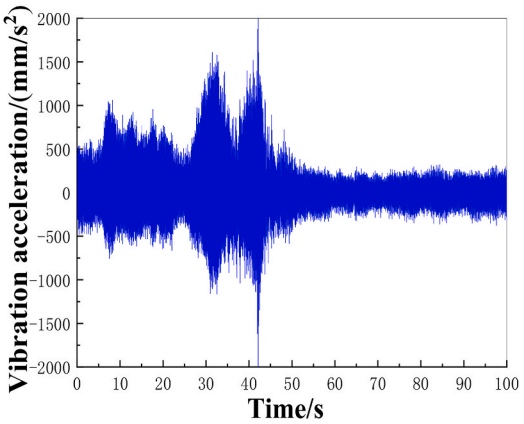

(a) Time course curve of vibration signal in Y direction of 1 # measuring point

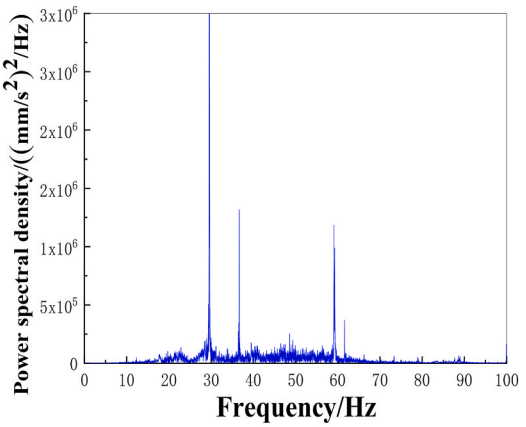

(b) Power spectrum density plot of vibration signal in Y direction of 1 # measuring point

Fig. 17. The time course and power spectrum density graph of vibration signal in Y direction of 1 # measuring point.

appearing in each IMF can be removed by the SVD algorithm, and IMF6 is used as an example to show the signal after SVD processing. The time course diagram and power spectrum density diagram of the signal after SVD processing are shown in Fig. 21.

From Fig. 21(a), it can be found that the waveform of the processed signal is clearer. Fig. 21(b) shows that the SVD method can extract signal features effectively, the main feature frequency 59.0 Hz of IMF6 is retained and other interference frequencies are effectively removed. The Y-direction signal of measurement point 1 after noise reduction is obtained by reconstructing the noise-reduced components of the SVD. The comparison of the Y-direction signal of measurement point 1 before and after noise reduction is shown in Fig. 22.

According to Fig. 22(a), although the original signal acquired in the Y direction at measurement point 1 is processed with noise reduction, it has little effect on the signal amplitude, the signal waveform and most of the peaks in the time-range diagram are still retained after noise reduction, and the signal characteristics are basically complete. With the help of EWT-SVD joint feature extraction method, the mixed interference signals in the vibration signal are filtered out, and the main energy signal is not lost. According to Fig. 22(b), it can be found that the spectrum density curve after noise reduction removes the interference signals distributed in the original signal between 10 and 100 Hz and with lower peaks, and retains the main frequencies 29.5 Hz, 36.5 Hz and 59.0 Hz of the signal.

Combining pipeline vibration signal analysis results with pipeline unit operations, it is evident that the feature extraction algorithm

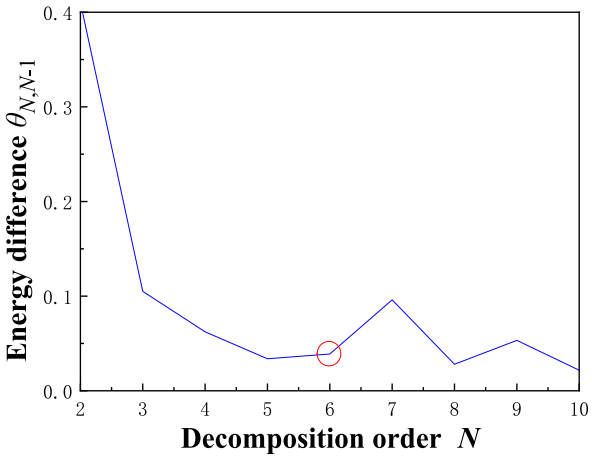

Fig. 18. Total energy difference curve of the $\theta_{N,N-1}$ of original signal.

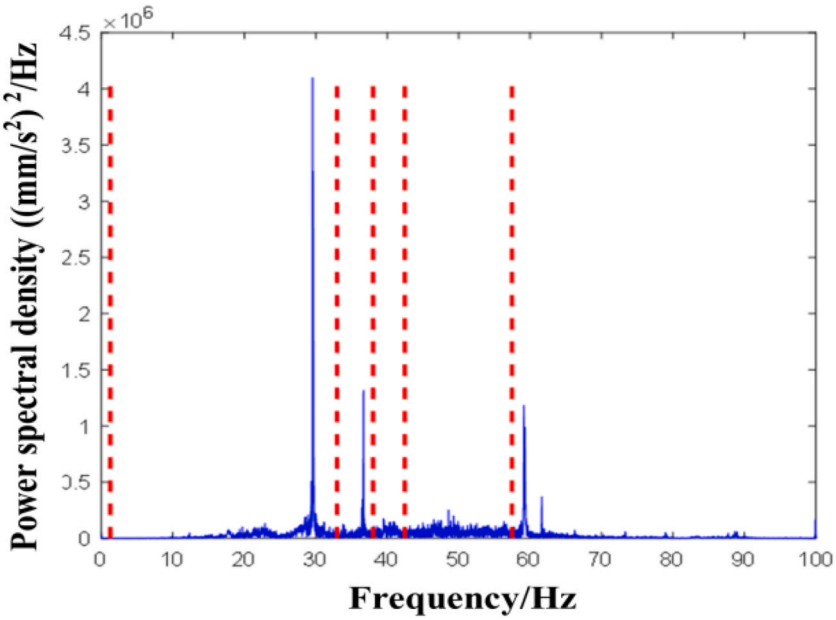

Fig. 19. Frequency domain division result of the original signal.

based on EWT effectively identifies the vibration characteristics of actual projects. This verifies the accuracy and practical engineering value of the EWT algorithm in signal analysis. The EWT method can further analyze pipeline vibration characteristics.

4.4. Characteristics of vibration sources for the dike crossing pipeline

In Section 4.2, the main vibration sources of the pipe vibration are identified as 29.5 Hz, 36.5 Hz, and 59.0 Hz. In Section 4.3, the EWT method is used to extract the characteristic frequencies of the signals at each measurement point and to filter out the interference signals. In order to obtain the vibration source characteristics of the pipeline, this section analyzes the time domain vibration of the vibration source based on the feature information extracted signals.

Considering that measurement points 1 and 2 exhibit the most intense vibrations, with the strongest vibration directions being the Y direction during shutdown, the X direction during startup, and the X direction during normal operation, the vibration source characteristics of the dike crossing pipeline are analyzed using the strongest vibration direction signals from these points as examples.

4.4.1. Shutdown condition

Yang'er water plant piping system using slow closing check valves to reduce the phenomenon of water hammer and prevent the backflow of water in the pipe. When the valve starts to close, 70–80 % of the valve is closed within 2–7 s, and then the valve is

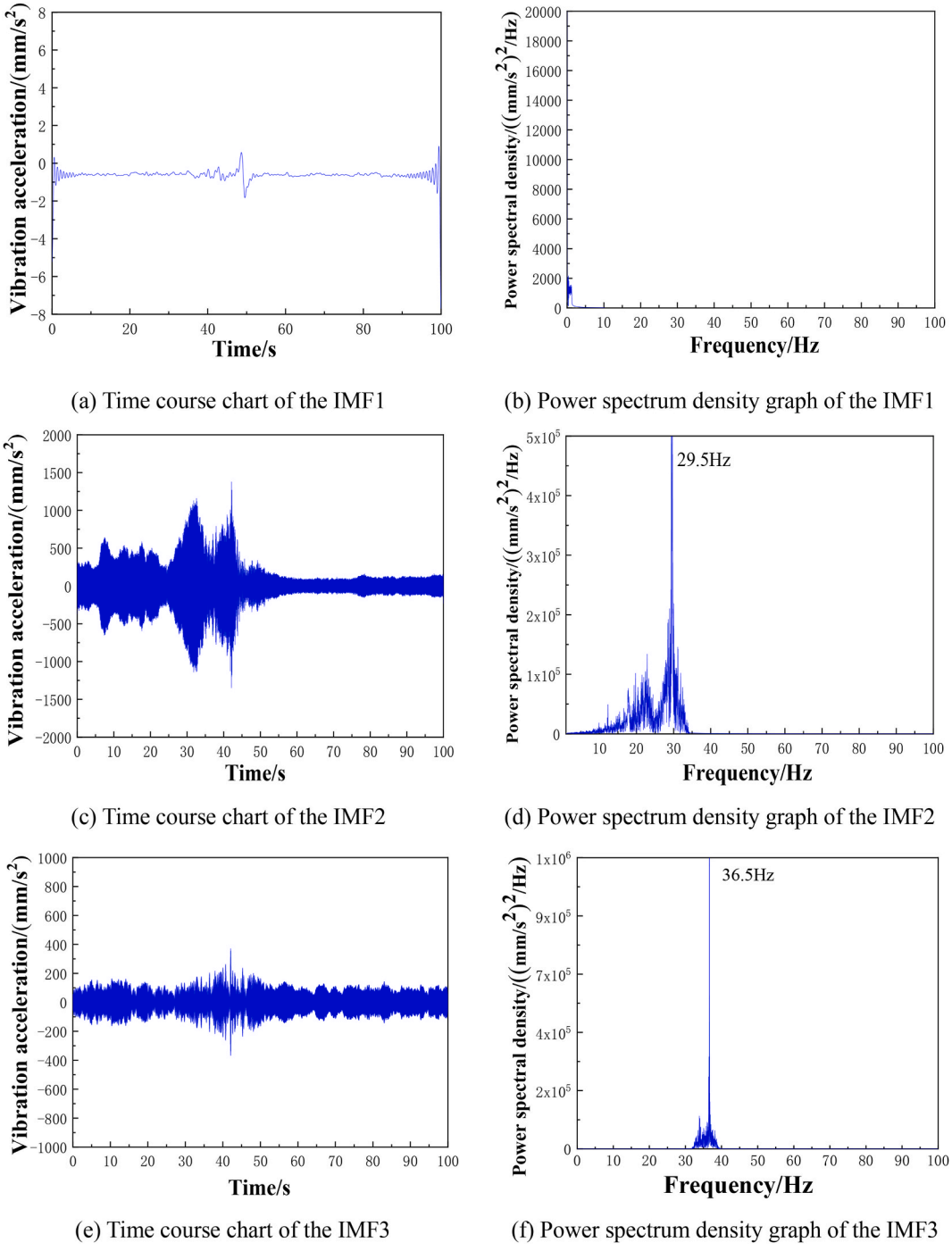

Fig. 20. Time course chart and power spectrum density graph of the IMF based on EWT.

completely closed according to the actual situation of the water supply network and the internal pressure of the pump. 6# pipe unit shutdown from 30s in shutdown condition. In order to refine the analysis of the pipeline shutdown process and identify the influence characteristics of the vibration source, the time-wavelet scale spectrum for the Y-direction signals of measurement point 1 and Y-direction signals of measurement point 2 under the shutdown condition are taken as examples, as shown in Figs. 23 and 24.

As shown in Figs. 23 and 24, the multiple rotational frequency 29.5 Hz is the main cause of pipe vibration. In the time-wavelet scale spectrum of the two measurement points, 29.5 Hz reaches the peak energy at 32.5s and 42.5s, which has the largest vibration energy. Besides, the energy corresponding to the leaf frequency of 59.0 Hz gets peaked at 42.5 s in the time-wavelet scale spectrum, and the

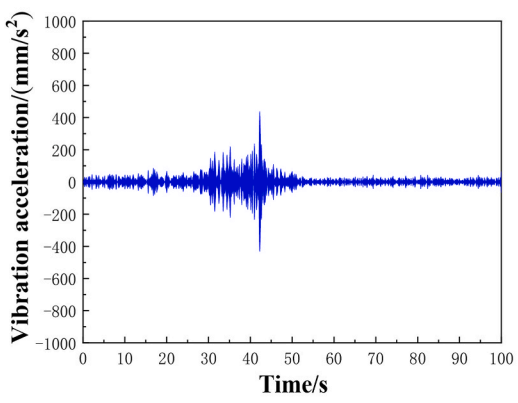

(g) Time course chart of the IMF4

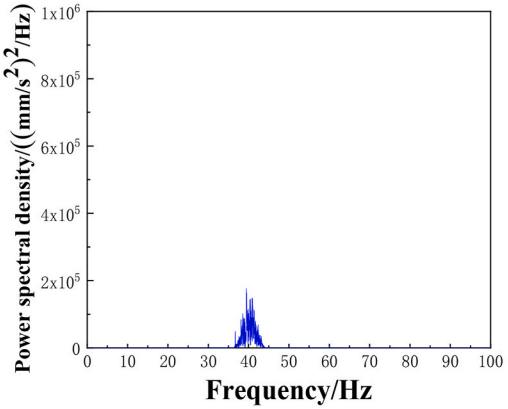

(h) Power spectrum density graph of the IMF4

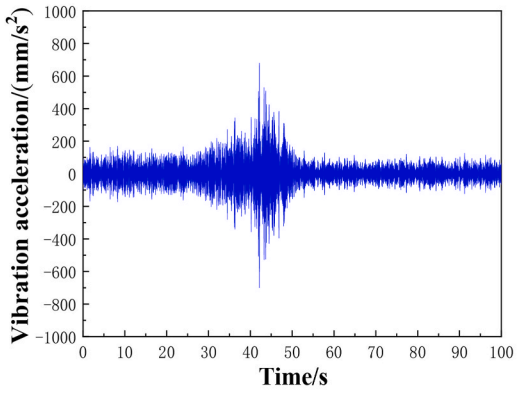

(i) Time course chart of the IMF5

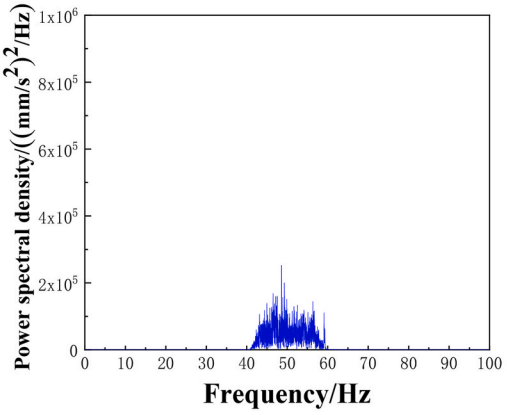

(j) Power spectrum density graph of the IMF5

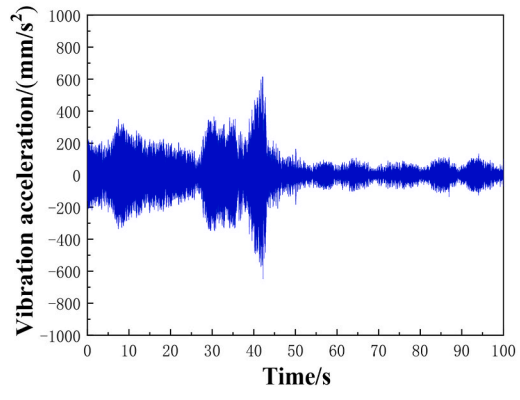

(k) Time course chart of the IMF6

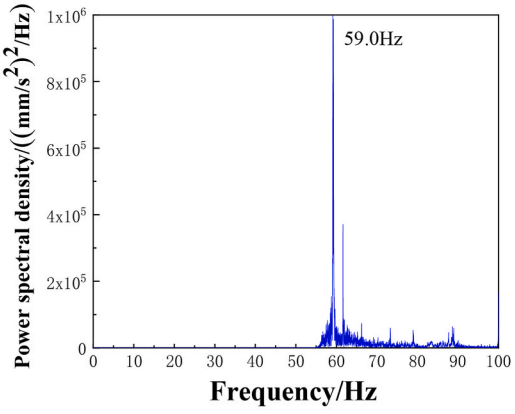

(l) Power spectrum density graph of the IMF6

Fig. 20. (*continued*).

energy is no longer highlighted after 44.5 s, which corresponds to the valve close of the pipeline shutdown condition. The pipeline unit starts to shutdown at 30s, and the time-wavelet scale spectrum of the measurement points shows obvious energy peaks at 32.5s and 42.5s due to the influence of the shutdown process. 32.5s corresponds to the first shutdown of the pipeline slow-closing check valve, 42.5s corresponds to the second shutdown of the pipeline slow-closing check valve, and the shutdown process is completed when the 6# pipeline unit stopped at 44.5s. The whole shutdown process took 14.5s.

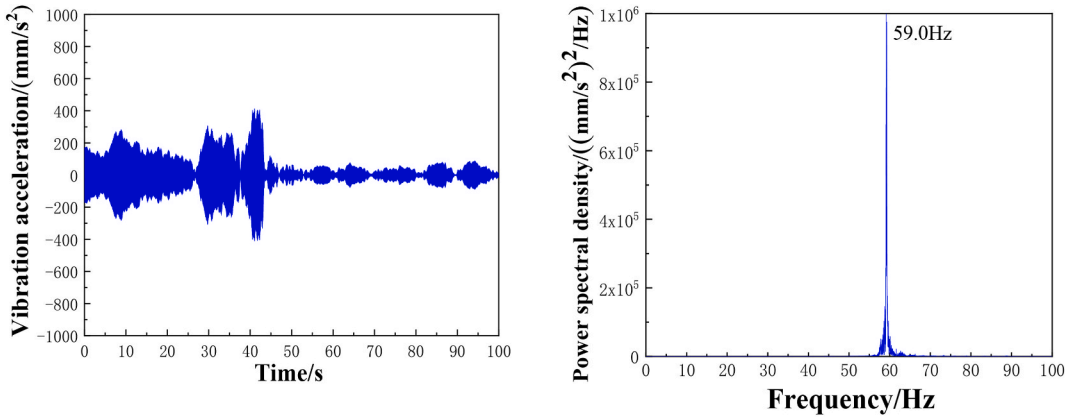

(a) Time course chart of the IMF6 after SVD denoising

(b) Power spectrum density graph of the IMF6 after SVD denoising

Fig. 21. Time course chart and power spectrum density graph of the IMF6 after SVD denoising.

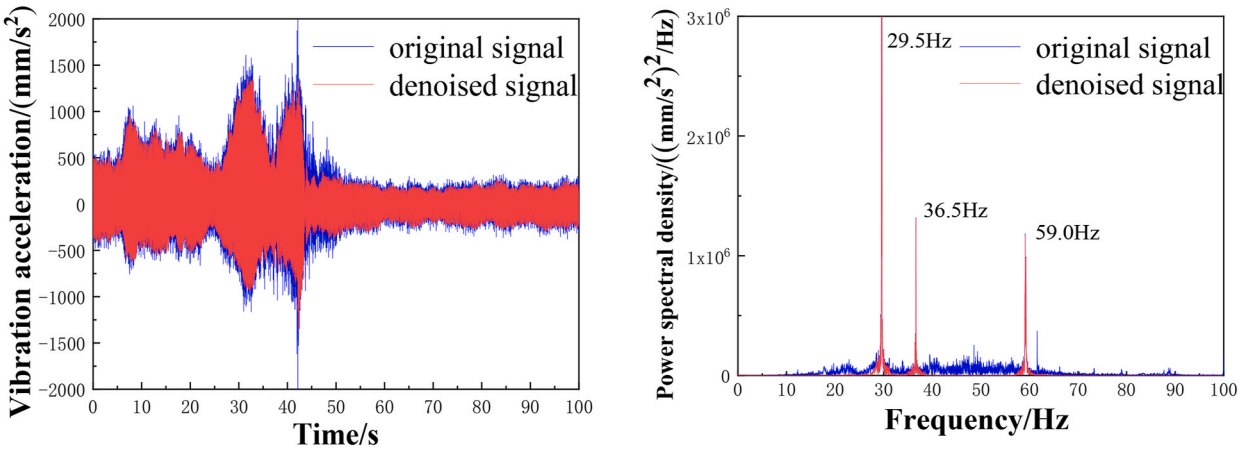

(a) Time course graph before and after noise reduction of Y-direction signal at measurement point 1

(b) Power spectrum density graph before and after noise reduction of Y-direction signal at measurement point 1

Fig. 22. Comparison of the time course and power spectrum density graph of Y-direction signal at measurement point 1.

4.4.2. Startup condition

Under the startup condition, the 6# pipeline unit begins to startup at 10s. In order to prevent cavitation, according to the operation of the pumping unit, the outlet valve is opened to complete the startup process after the unit speed is stable. The influence of vibration sources under the startup condition of the 6# pipeline unit is analyzed, and the time-wavelet scale spectrum of the signals in the X-direction of measurement point 1 and measurement point 2 under the startup condition are shown in Figs. 25 and 26.

Analyzing the time-wavelet scale spectrum of the X-direction measurement points under the startup condition, the energies of 29.5 Hz, 36.5 Hz, and 59.0 Hz appear in all time domains. Since 36.5 Hz is caused by the neighboring unit of the 7# pipeline and is not directly generated by the 6# pipeline unit, the energy is lower than 29.5 Hz and there is no obvious energy peak in the time domain.

Comprehensive analysis of the time-wavelet scale spectrum of the measurement point signals under the startup condition, the pipeline unit begins to startup at 10s, as the unit continues to run, the 29.5 Hz rotational frequency energy continues to increase, the 29.5 Hz rotational frequency energy appears a peak and the leaf frequency energy of 59.0 Hz increases significantly at 29s, which corresponds to the state of the pipeline outlet valve is open, and the unit startup is completed. After 29s, the pipeline enters the normal operation state, and the vibration energy of the pipeline is higher than that before the unit is startup. The analysis results based on the time-wavelet scale spectrum correspond to the real characteristics of the pipeline operation, which objectively reflects the vibration

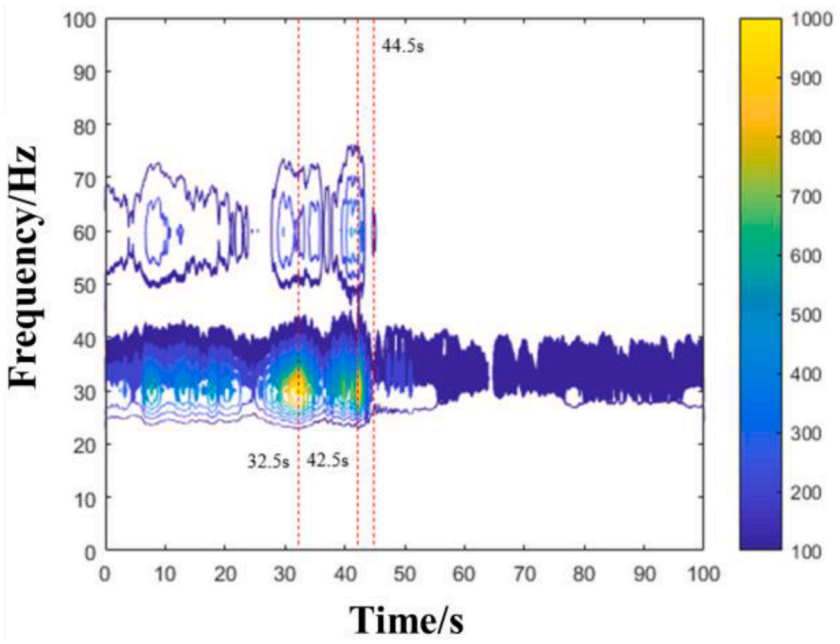

Fig. 23. Time-wavelet scale spectrum of Y-direction signal at measurement point 1.

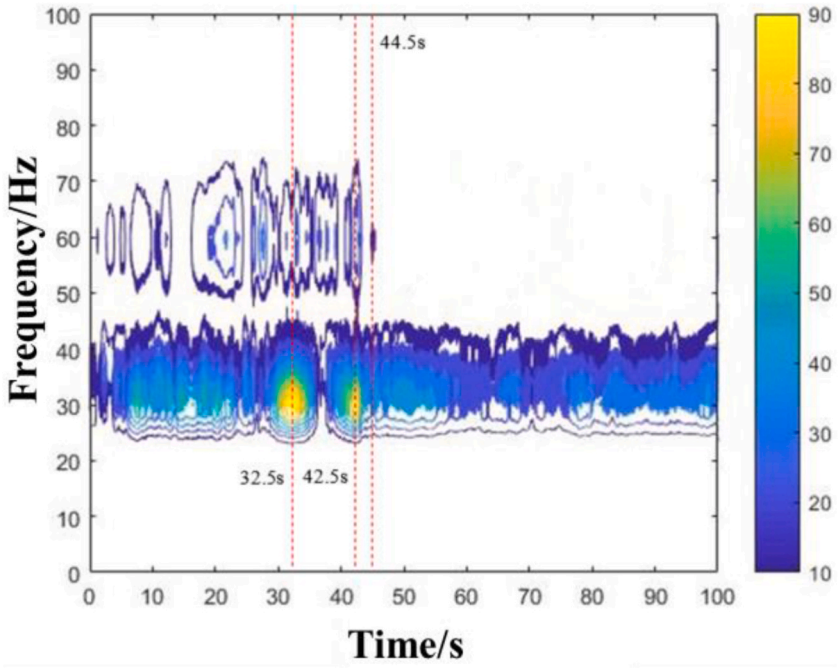

Fig. 24. Time-wavelet scale spectrum of Y-direction signal at measurement point 2.

process of the pipeline under the startup condition.

4.4.3. Normal operation condition

The time-wavelet scale spectrum of the signals in the X-direction at measurement point 1 and measurement point 2 under normal operation condition are shown in Figs. 27 and 28.

As can be seen from Figs. 27 and 28, under normal operation condition, the pipe vibration has no obvious energy change characteristics, the vibration energy is relatively equal in the entire time domain, the vibration energy of each measurement point is 29.5

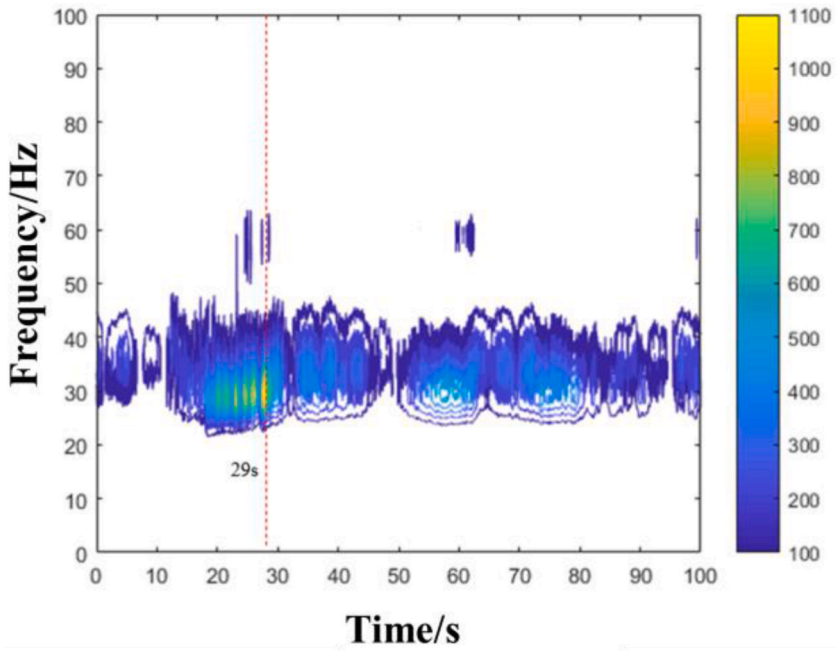

Fig. 25. Time-wavelet scale spectrum of X-direction signal at measurement point 1.

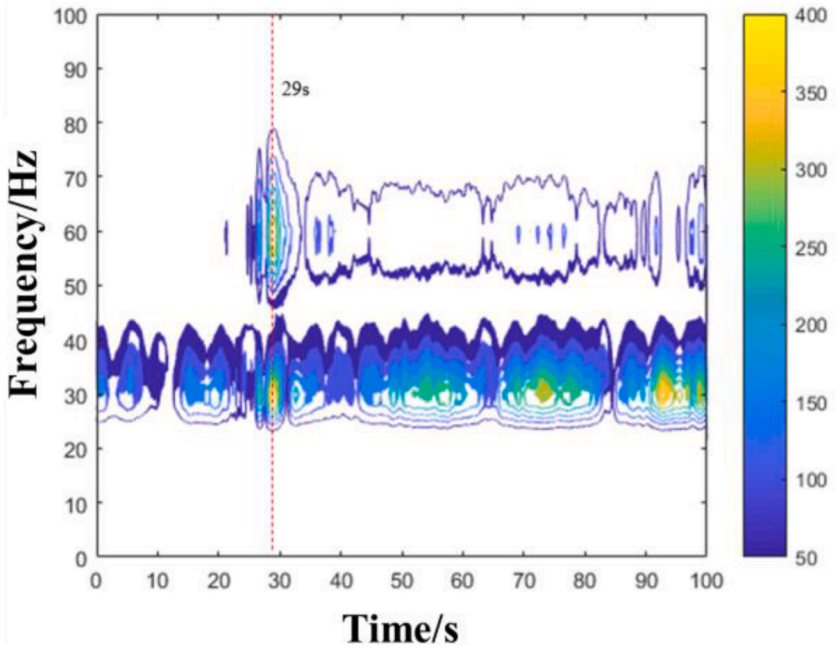

Fig. 26. Time-wavelet scale spectrum of X-direction signal at measurement point 2.

Hz, 36.5 Hz, 59.0 Hz, these frequencies are distributed throughout the entire time domain; The highest energy is 29.5 Hz, indicating that the vibration at the measurement point is mainly caused by multiple rotational frequency of unit.

4.5. Coupled vibration characteristics for the dike crossing pipeline

Using the time-wavelet scale spectrum, the strong moments and energy characteristics of the vibration source during pipeline operation under various conditions are effectively analyzed, clarifying the influence of multiple rotational and leaf frequencies in the

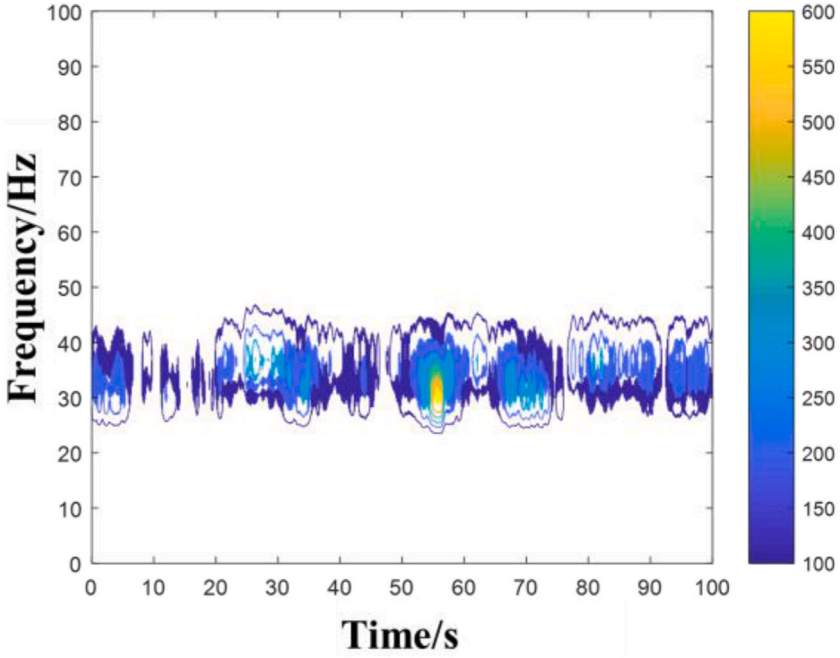

Fig. 27. Time-wavelet scale spectrum of X-direction signal at measurement point 1.

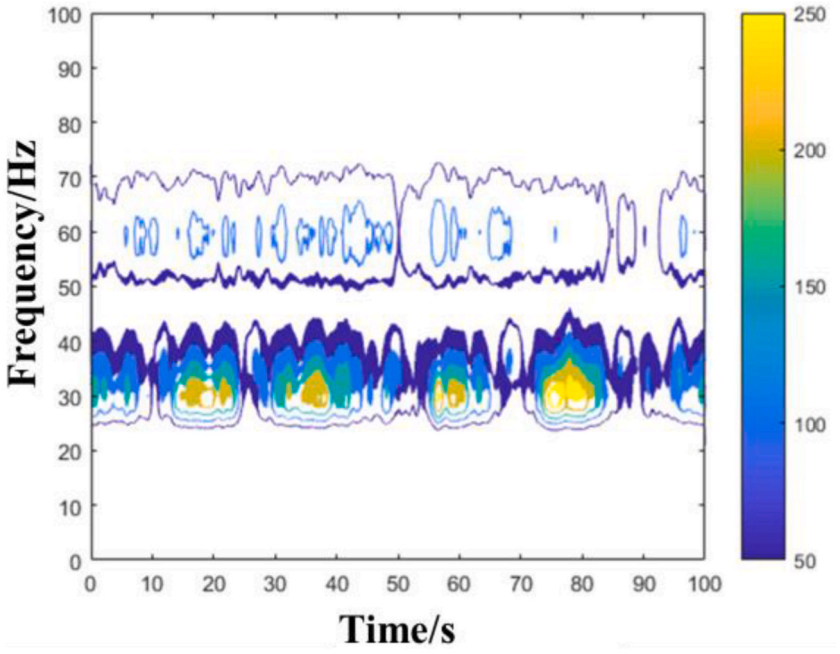

Fig. 28. Time-wavelet scale spectrum of X-direction signal at measurement point 2.

time domain. However, the effect of different vibration sources on pipeline measurement points varies with operating conditions, and each measurement point exhibits unique structural characteristics and interactions. Therefore, studying the coupled vibration characteristics between different measurement points is essential. This section analyzes the coupled vibration characteristics of the measurement points under shutdown condition, startup condition and normal operation condition with the help of cross wavelet transform method. The cross time-wavelet scale spectrum of the Y-direction signals of measurement point 1 and measurement point 2 under the shutdown condition, the cross time-wavelet scale spectrum of the X-direction signals of measurement point 1 and measurement point 2 under the startup condition, and the cross time-wavelet scale spectrum of the X-direction signals of measurement

point 1 and measurement point 2 under the normal operation condition are shown in Fig. 29(a–c).

As can be seen from Fig. 29(a–c), measurement point 1 and measurement point 2 show strong correlation throughout the startup and shutdown conditions. During the shutdown condition from 30s to 44.5s, the cross-time-wavelet scale spectrum achieves an energy peak at 32.5s, indicating that the coupled vibration of the measurement points is strongest at that moment. Similarly, during the startup condition from 10s to 29s, the cross time-wavelet scale spectrum obtains the energy peak at 29s, indicating that the coupled vibration of the measurement point is strongest at 29s.

Combined with the preceding analysis, the results of cross wavelet transform are consistent with the operation law of the dike crossing pipeline, and can show the coupled vibration energy peaks in the corresponding time, which further identifies the relevant vibration characteristics of the dike crossing pipeline. The peak value of vibration energy of 6# pipeline under shutdown condition, startup condition and normal operation condition is concentrated at 29.5 Hz, indicating that the source of coupled vibration for the dike crossing pipeline is the multiple rotational frequency of the 6# pipeline unit.

5. Discussion

In this study, we propose an EWT-CWT based method for analyzing the coupled vibration characteristics of the dike crossing pipeline to achieve a comprehensive understanding of pipeline vibration characteristics. With reference to the literature [44–47], the application of the research method in other fields and the application of the EWT-CWT coupling vibration analysis method are discussed in this section in order to fully illustrate the rationality and wide applicability of the method in this paper.

The signals collected from engineering structures often contain various noise components, necessitating effective methods to extract feature information. This paper primarily involves two steps: correlation frequency identification and main vibration source extraction. The mutual correlation analysis is a method used to analyze the correlation of two or more signals in the frequency domain. By employing this technique, we can identify the correlation frequency components within the signals, which represent the main sources of vibration. EWT is an adaptive signal analysis tool particularly suited for non-stationary and multi-component signal analysis [36–39]. By decomposing the signal into multiple frequency bands using the EWT method and extracting the main vibration sources in each band, a foundation is laid for subsequent analysis of vibration source characteristics.

Fourier transform is a widely used technique in signal processing and vibration analysis, capable of converting time-domain signals into frequency-domain signals, thereby revealing the frequency components within the signal [48]. Traditional structural vibration analysis typically employs Fourier transform for vibration source identification and frequency domain feature analysis [33,38,43]. However, its main limitation lies in providing global frequency information rather than local or time-domain information. This means that while we can determine the presence of a frequency component over the entire time period, we cannot directly discern its specific impact range in the time domain from the Fourier transform results. In the simulation analysis section, we have discussed this limitation may pose in practical applications. From the perspective of comprehensively and deeply identifying vibration source characteristics, Fourier transform is not the optimal choice.

To address this issue, this paper employs the Wavelet Transform method for analyzing the time-domain characteristics of main vibration sources. When analyzing the vibration of a single component, Wavelet Transform effectively identifies and separates vibration characteristics at different time and frequency scales, clearly pinpointing which parts of the structure exhibit significant vibrations at specific frequencies and time points [18–20]. However, for a large, complex system involving multiple components, vibration issues often extend beyond a single part and involve interactions and influences between components. In such cases, analyzing the vibration characteristics of a single part may not fully reveal the system's dynamic behavior, nor can it capture the core coupled vibration of the entire system.

CWT is a method for analyzing the interrelationship between two time series, particularly suited for examining the interactions of

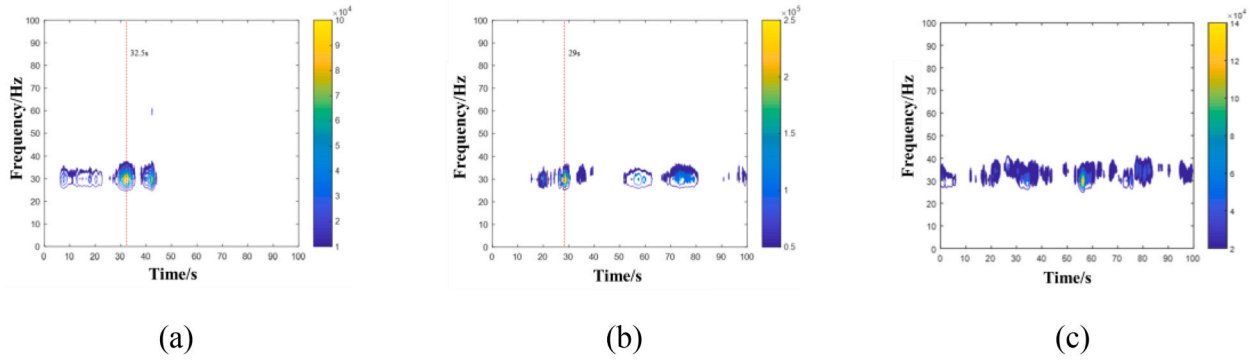

Fig. 29. Cross time-wavelet scale spectrum of different working conditions
(a) Cross time-wavelet scale spectrum between measurement point 1 and measurement point 2 of Y direction signal under shutdown condition
(b) Cross time-wavelet scale spectrum between measurement point 1 and measurement point 2 of X direction signal under startup condition
(c) Cross time-wavelet scale spectrum between measurement point 1 and measurement point 2 of X direction signal under the normal operation condition.

nonlinear and non-stationary signals. Swati [49] applied CWT to two ECG time series and cross-checked the two series, revealing local similarities in time and frequency. Aslak [50] applied CWT to the Arctic Oscillation index and the Baltic Sea maximum ice extent records to validate the method's effectiveness in analyzing the time-frequency space between two time series. Li [51] studied the propagation time of agricultural drought using cross wavelet analysis.

In summary, EWT is an effective method for extracting main vibration sources, CWT can effectively analyze the coupling characteristics between related signals. The pipeline is influenced by various vibration sources such as multiple rotational frequency and the leaf frequency, which have different time-domain impacts and affect different parts of the structure. These sources exhibit both temporal and spatial characteristics, potentially propagating and interacting within the pipeline structure to form complex coupled vibration patterns. By employing EWT-CWT, we can accurately analyze these vibrational interactions in both time and frequency domains, identifying core vibration sources through phenomenon such as frequency synchronization and energy concentration. The study identifies the multiple rotational frequency of the 6# pipeline unit (29.5Hz) as the core source of coupled vibrations. Combining EWT and CWT methods based on prototype observation data for analyzing coupled vibration characteristics of pipelines leverages the strengths of both methods, yielding optimal results. This approach is highly innovative and theoretically feasible in the field of pipeline vibration research.

This research provides a systematic analysis framework for structural coupled vibrations, contributing significantly to scientific research and technological advancements in the field of structural vibrations. The study's methodologies are not only applicable to dike crossing pipelines but also to other structures such as bridges, buildings, and mechanical equipment. It effectively aids researchers in more efficient structural design and maintenance, offering high practical value and potential for widespread application.

Currently, this study is primarily based on prototype observation data, utilizing the EWT-CWT method to effectively extract the coupled vibration characteristics of dike crossing pipelines. Although the results derived from real-world data are accurate and reliable, there are still areas for improvement in the analysis of pipeline coupled vibration characteristics. Numerical simulation has become a common method for analyzing pipeline flow-induced vibrations. Liang [52] considered the interaction between fluid (e.g., water) and pipeline structure. Through FSI analysis, they identified the dynamic variations of pipeline vibrations caused by gas-liquid two-phase flow in bends. Kun [53] studied fluid-acoustic-structure coupled vibrations in nuclear power plants, using computational fluid dynamics (CFD) analysis and Strouhal number calculations to verify that fluid-acoustic-structure coupling is the fundamental cause of stagnant branch pipeline vibrations. Liu [54] employed CFD to establish discrete phase models (DPM) and erosion wear models (EWM), investigating the erosion effects on pipelines under different conditions and proposing optimization measures for pipeline protection.

Prototype observation data reflect the vibration behavior of pipelines in real working environments and provide a basis for validating and calibrating numerical models. Numerical simulations can model the sensitivity parameters of prototypes, identifying more complex and comprehensive coupled vibration characteristics. Combining prototype observation data with numerical simulation analysis will be a new direction for future research on pipeline coupled vibration characteristics.

6. Conclusion

This paper explores a vibration characteristics identification method based on EWT and CWT, verifies the effectiveness of the algorithm through simulation signal analysis, analyzes the vibration source characteristics and coupled vibration characteristics of the dike crossing pipeline, and obtains the following conclusions.

(1) According to the results of the mutual correlation power spectrum analysis, the multiple rotational frequency 29.5 Hz, 36.5 Hz and the leaf frequency 59.0 Hz of the 6# pipeline unit have the highest energy and appear the most times, indicating that the two vibration sources are the main factors leading to pipeline vibration and there is a certain degree of correlation between each point.
(2) Through the analysis of simulation signals, it is clear that the EWT parameter optimization method can effectively identify the optimal decomposition order N, and the EWT algorithm can effectively extract the signal characteristic frequency. According to the signals of the dike crossing pipeline, the vibration characteristic frequencies 29.5 Hz, 36.5 Hz and 59.0 Hz are extracted with the help of the EWT method. It is found that the EWT method can effectively remove the interfering signals and extract the signal feature information, which lays the foundation for the subsequent research and provides new ideas for similar engineering analyses.
(3) Analyzing the time-domain characteristics of vibration sources of dike crossing pipeline using time-wavelet scale spectrum. The pipeline unit starts to shutdown at 30s, and the time-wavelet scale spectrum of the measurement points shows obvious energy peaks at 32.5s and 42.5s due to the influence of the shutdown process. 32.5s corresponds to the first shutdown of the pipeline slow-closing check valve, 42.5s corresponds to the second shutdown of the pipeline slow-closing check valve, and the shutdown process is completed when the 6# pipeline unit stopped at 44.5s. The pipeline unit begins to startup at 10s, as the unit continues to run, the multiple rotational frequency energy of 29.5 Hz appears a peak and the leaf frequency energy of 59.0 Hz increases significantly at 29s, which corresponds to the state of the pipeline outlet valve open and the unit startup is completed.
(4) Analyzing the coupled vibration characteristics of the dike crossing pipeline based on the cross wavelet transform, the peak energy of the coupled vibration of the 6# pipeline is generally concentrated at the frequency of 29.5 Hz, and the source of the coupled vibration is the multiple rotational frequency of the 6# pipeline unit.

Currently, this study primarily relies on prototype observation data, utilizing the EWT-CWT method to effectively extract the

coupled vibration characteristics of dike crossing pipeline, which heavily depends on the quality of the observation data. Noise or incompleteness in the data may potentially affect the accuracy of the analysis results. It should be noted that numerical simulation has become a common method for analyzing pipeline flow-induced vibrations. In the future, combining prototype observation data with numerical simulation analysis will be a new direction for research on pipeline coupled vibration characteristics and vibration mitigation for safety.

Funding

The authors are grateful for the financial support from the National Natural Science Foundation of China (52279133), the Science and Technology Innovation Program from Water Resources of Guangdong Province (2024-07) and the Innovative Project of North China University of Water Resources and Electric power (YK-2021-30). The findings and opinions expressed in this paper are solely of the authors and do not represent the views of the sponsors.

Institutional review board statement

Not applicable.

Informed consent statement

Not applicable.

Data availability statement

The data associated with this study have not been deposited into a publicly available repository. The data associated with this study will be made available on request.

CRediT authorship contribution statement

Jinlin Huang: Writing – review & editing, Visualization, Investigation, Data curation. **Ziyu Li:** Writing – review & editing, Writing – original draft, Software, Methodology, Data curation, Conceptualization. **Jianwei Zhang:** Resources, Investigation, Funding acquisition, Data curation.

Declaration of competing interest

The authors declare that they have no known competing financial interests or personal relationships that could have appeared to influence the work reported in this paper.

Acknowledgement

The authors are grateful for the financial support from the National Natural Science Foundation of China (52279133), the Science and Technology Innovation Program from Water Resources of Guangdong Province (2024-07) and the Innovative Project of North China University of Water Resources and Electric power (YK-2021-30).

References

[1] F. Wang, J. Shao, W. Li, Y. Wang, L. Wang, H. Liu, Study on the effect of pile foundation reinforcement of embankment on slope of soft soil, Sustainability 14 (21) (2022) 14359, https://doi.org/10.3390/su142114359.
[2] J. Yu, J. Liu, Z. Jiang, X. Kang, Analysis of the influence of whipstock point position of direction drilling through embankment on the stability of embankment slope against sliding, Adv. Civ. Eng. 2022 (2022) 296402, https://doi.org/10.1155/2022/2296402.
[3] D. Lu, G. Cong, B. Li, A new risk assessment model to check safety threats to long-distance pipelines, J. Press. Vess-T. Asme. 144 (5) (2022) 051801, https://doi.org/10.1115/1.4052064.
[4] Y. Liu, X. Dai, J. Qi, M. Xu, J. Zhang, F. Yang, X. He, Vibration characteristics of pipe based on panoramic amplitude-fluctuation electronic speckle pattern interferometry, Measurement 202 (2022) 111802, https://doi.org/10.1016/j.measurement.2022.111802.
[5] J.X. Liu, T.Y. Li, T.G. Liu, J. Yan, Vibration characteristic analysis of buried pipes using the wave propagation approach, Appl. Acoust. 66 (3) (2005) 353–364, https://doi.org/10.1016/j.apacoust.2004.06.010.
[6] X. Guo, P. Gao, H. Ma, H. Li, B. Wang, Q. Han, B. Wen, Vibration characteristics analysis of fluid-conveying pipes concurrently subjected to base excitation and pulsation excitation, Mech. Syst. Signal Process. 189 (2023) 110086, https://doi.org/10.1016/j.ymssp.2022.110086.
[7] L. Quan, S. Che, C. Guo, H. Gao, M. Guo, Axial vibration characteristics of fluid-structure interaction of an aircraft hydraulic pipe based on modified friction coupling model, Appl. Sci-Basel. 10 (10) (2020) 3548, https://doi.org/10.3390/app10103548.
[8] N. Jiang, B. Zhu, C. Zhou, H. Li, B. Wu, Y. Yao, T. Wu, Blasting vibration effect on the buried pipeline: a brief overview, Eng. Fail. Anal. 129 (2021) 105709, https://doi.org/10.1016/j.engfailanal.2021.105709.
[9] H. Zhang, M. Qin, K. Liao, K. Wang, G. He, Pipe-soil vibration characteristics of natural gas pipelines during the pigging process, J. Nat. Gas Sci. Eng. 95 (2021) 104148, https://doi.org/10.1016/j.jngse.2021.104148.
[10] H. Ding, J. Ji, L.Q. Chen, Nonlinear vibration isolation for fluid-conveying pipes using quasi-zero stiffness characteristics, Mech. Syst. Signal Process. 121 (2019) 675–688, https://doi.org/10.1016/j.ymssp.2018.11.057.

[11] L. Li, H. Cai, H. Han, Q. Jiang, H. Ji, Adaptive short-time Fourier transform and synchrosqueezing transform for non-stationary signal separation, Signal Process. 166 (2020) 107231, https://doi.org/10.1016/j.sigpro.2019.07.024.
[12] D. Jana, S. Nagarajaiah, Computer vision-based real-time cable tension estimation in Dubrovnik cable-stayed bridge using moving handheld video camera, Struct. Control Health Monit. 28 (5) (2021) e2713, https://doi.org/10.1002/stc.2713.
[13] H. Chen, Z. Dang, S.S. Park, R. Hugo, Robust CNN-based flow pattern identification for horizontal gas-liquid pipe flow using flow-induced vibration, Exp. Therm. Fluid Sci. 2023 (148) (2023) 110979, https://doi.org/10.1016/j.expthermflusci.2023.110979.
[14] H. Jeon, Y. Jung, S. Lee, Y. Jung, Area-efficient short-time fourier transform processor for time–frequency analysis of non-stationary signals, Appl. Sci-Basel. 10 (20) (2020) 7208, https://doi.org/10.3390/app10207208.
[15] L. Bykerk, J.M. Valls, Vibro-acoustic distributed sensing for large-scale data-driven leak detection on urban distribution mains, Sensors 22 (18) (2022) 6897, https://doi.org/10.3390/s22186897.
[16] W.J. Staszewski, G.R. Tomlinson, Application of the wavelet transform to fault detection in a spur gear, Mech. Syst. Signal Process. 8 (3) (1994) 289–307, https://doi.org/10.1006/mssp.1994.1022.
[17] C. Tian, M. Zheng, W. Zuo, B. Zhang, Y. Zhang, D. Zhang, Multi-stage image denoising with the wavelet transform, Pattern, Recogn 134 (2023) 109050, https://doi.org/10.1016/j.patcog.2022.109050.
[18] T. Wang, C. Lu, Y. Sun, M. Yang, C. Liu, C. Ou, Automatic ECG classification using continuous wavelet transform and convolutional neural network, Entropy 23 (1) (2021) 119, https://doi.org/10.3390/e23010119.
[19] Y. Liu, L. Guan, C. Hou, H. Han, Z. Liu, Y. Sun, M. Zheng, Wind power short-term prediction based on LSTM and discrete wavelet transform, Appl. Sci-Basel. 9 (6) (2019) 1108, https://doi.org/10.3390/app9061108.
[20] R. Perna, M. Abela, M. Mameli, A. Mariotti, L. Pietrasanta, M. Marengo, S. Filippeschi, Flow characterization of a pulsating heat pipe through the wavelet analysis of pressure signals, Appl. Therm. Eng. 171 (2020) 115128, https://doi.org/10.1016/j.applthermaleng.2020.115128.
[21] A. Kyprianou, W.J. Staszewski, On the cross wavelet analysis of Duffing oscillator, J. Sound Vib. 228 (1) (1999) 199–210, https://doi.org/10.1006/jsvi.1999.2420.
[22] T. Pagliaroli, F. Gambioli, F. Saltari, J. Cooper, Proper orthogonal decomposition, dynamic mode decomposition, wavelet and cross wavelet analysis of a sloshing flow, J. Fluid Struct. 112 (2022) 103603, https://doi.org/10.1016/j.jfluidstructs.2022.103603.
[23] J.T. Ellis, D.J. Sherman, Cross-wavelet analysis of coherent wind and saltation events, Earth. Surf. Proc. Land. 48 (2) (2023) 406–414, https://doi.org/10.1002/esp.5493.
[24] P. Dhar, S. Dutta, V. Mukherjee, Cross-wavelet assisted convolution neural network (AlexNet) approach for phonocardiogram signals classification, Biomed. Signal Process Control 63 (2021) 102142, https://doi.org/10.1016/j.bspc.2020.102142.
[25] H. Li, B. Liu, W. Huang, H. Liu, G. Wang, Vibration load identification in the time-domain of high arch dam under discharge excitation based on hybrid LSQR algorithm, Mech. Syst. Signal Process. 177 (2022) 109193, https://doi.org/10.1016/j.ymssp.2022.109193.
[26] N.E. Huang, Z. Shen, S.R. Long, M.C. Wu, H.H. Shih, Q. Zheng, et al., The empirical mode decom-position and the Hilbert spectral for nonlinear and non-stationary time series analysis, Proceedings of the Royal Society of London. Series A: Math. Phys. Eng. Sci. 454 (1998) 903–995, https://doi.org/10.1098/rspa.1998.0193, 1971.
[27] N.E. Huang, Z. Shen, S.R. Long, A new view of nonlinear water waves: the Hilbert spectral, Annu. Rev. Fluid Mech. 31 (1999) 417–457, https://doi.org/10.1146/annurev.fluid.31.1.417.
[28] M. Barbosh, P. Singh, A. Sadhu, Empirical mode decomposition and its variants: a review with applications in structural health monitoring, Smart, Mater. Struct. 29 (9) (2020) 093001, https://doi.org/10.1088/1361-665x/aba539.
[29] F. Bolaers, O. Cousinard, P. Estocq, X. Chiementin, J.P. Dron, Comparison of denoising methods for the early detection of fatigue bearing defects by vibratory analysis, J. Vib. Control 17 (13) (2011) 1983–1993, https://doi.org/10.1177/1077546309348853.
[30] G. Gai, The processing of rotor startup signals based on empirical mode decomposition, Mech. Syst. Signal Process. 20 (1) (2006) 222–235, https://doi.org/10.1016/j.ymssp.2004.07.001.
[31] Y. Zhang, J.J. Lian, G.X. Zhang, Y. Liu, M.M. Song, S.H. Li, Ground vibration characteristics induced by flood discharge of a high dam: an experimental investigation, J. Renew. Sustain. Ener. 13 (13) (2021) 1–17, https://doi.org/10.1063/5.0019214.
[32] Z. Wu, N.E. Huang, Ensemble empirical mode decomposition: a noise-assisted data analysis method, Adv. Adapt. Data Anal. 1 (1) (2009) 1–41, https://doi.org/10.1142/s1793536909000047.
[33] Y. Zhang, J. Lian, F. Liu, An improved filtering method based on EEMD and wavelet-threshold for modal parameter identification of hydraulic structure, Mech. Syst. Signal Process. 68 (2016) 316–329, https://doi.org/10.1016/j.ymssp.2015.06.020.
[34] Z. Gao, Y. Liu, Q. Wang, J. Wang, Y. Luo, Ensemble empirical mode decomposition energy moment entropy and enhanced long short-term memory for early fault prediction of bearing, Measurement 188 (2022) 110417, https://doi.org/10.1016/j.measurement.2021.110417.
[35] H. Wang, Z. Liu, Y. Song, X. Lu, Ensemble EMD-based signal denoising using modified interval thresholding, IET Signal Process. 11 (4) (2017) 452–461, https://doi.org/10.1049/iet-spr.2016.0147.
[36] J. Gilles, Empirical wavelet transform, IET, Signal Process. 61 (16) (2013) 3999–4010, https://doi.org/10.1109/TSP.2013.2265222.
[37] L. Peng, L. Wang, D. Xia, Q. Gao, Effective energy consumption forecasting using empirical wavelet transform and long short-term memory, Energy 238 (2022) 121756, https://doi.org/10.1016/j.energy.2021.12175.
[38] Q. Liu, J. Yang, K. Zhang, An improved empirical wavelet transform and sensitive components selecting method for bearing fault, Measurement 187 (2022) 110348, https://doi.org/10.1016/j.measurement.2021.110348.
[39] H. Yu, H. Li, Y. Li, Vibration signal fusion using improved empirical wavelet transform and variance contribution rate for weak fault detection of hydraulic pumps, ISA. T. 107 (2020) 385–401, https://doi.org/10.1016/j.isatra.2020.07.025.
[40] R. Liang, W. Liu, S. Kaewunruen, H. Zhang, Z. Wu, Classification of External vibration sources through data-driven models using hybrid CNNs and LSTMs, Struct. Control Health Monit. 2023 (2023) 1900447, https://doi.org/10.1155/2023/1900447.
[41] P. Toiviainen, M. Hartmann, Analyzing multidimensional movement interaction with generalized cross-wavelet transform, Hum. Movement. Sci. 81 (2022) 102894, https://doi.org/10.1016/j.humov.2021.102894.
[42] R.X. Dong, D.L. Zhou, Correlation function and mutual information, J. Phys. A-Math. Theor. 43 (44) (2010) 445302, https://doi.org/10.1088/1751-8113/43/44/445302.
[43] J. Zhang, Z. Li, J. Huang, M. Cheng, H. Li, Study on vibration-transmission-path identification method for hydropower houses based on CEEMDAN-SVD-TE, Appl. Sci-Basel. 12 (15) (2022) 7455, https://doi.org/10.3390/app12157455.
[44] Z. Wang, Y. Liu, C. Gong, Z. Yuan, L. Shen, P. Chang, K. Liu, T. Xu, J. Jiang, Y.C. Chen, T. Liu, Liquid crystal-amplified optofluidic biosensor for ultra-highly sensitive and stable protein assay, PhotoniX 2 (1) (2021) 18, https://doi.org/10.1186/s43074-021-00041-1.
[45] Y. Qi, Y. Liu, J. Luo, Recent application of Raman spectroscopy in tumor diagnosis: from conventional methods to artificial intelligence fusion, PhotoniX 4 (1) (2023) 22, https://doi.org/10.1186/s43074-023-00098-0.
[46] Z. Wang, G. Fang, Z. Gao, Y. Liao, C. Gong, M. Kim, G. Cheng, S. Feng, T. Xu, T. Liu, Y. Chen, Autonomous microlasers for profiling extracellular vesicles from cancer spheroids, Nano Lett. 23 (7) (2023) 2502–2510, https://doi.org/10.1021/acs.nanolett.2c04123.
[47] J. Jing, K. Liu, J. Jiang, T. Xu, L. Xiao, X. Zhan, T. Liu, Optimally configured optical fiber near-field enhanced plasmonic resonance immunoprobe for the detection of alpha-fetoprotein, Adv. Sci. 10 (15) (2023) 2207437, https://doi.org/10.1002/advs.202207437.
[48] H. Manus, An ultra-precise fast Fourier transform, Measurement 220 (2023) 113372, https://doi.org/10.1016/j.measurement.2023.113372.
[49] Ba Swati, M. Mitra, Application of cross wavelet transform for ECG pattern analysis and classification, IEEE. T. Instrum. Meas. 63 (2) (2013) 326–333, https://doi.org/10.1109/TIM.2013.2279001.
[50] G. Aslak, J. Moore, S. Jevrejeva, Application of the cross wavelet transform and wavelet coherence to geophysical time series, Nonlinear, Proc. Geoph. 11 (5/6) (2004) 561–566, https://doi.org/10.5194/npg-11-561-2004.

[51] R. Li, N. Chen, X. Zhang, L. Zeng, X. Wang, S. Tang, D. Li, D. Niyogi, Quantitative analysis of agricultural drought propagation process in the Yangtze River Basin by using cross wavelet analysis and spatial autocorrelation, Agr. Forest. Meteorol 280 (2020) 107809, https://doi.org/10.1016/j.agrformet.2019.107809.
[52] Z. Liang, C. Guo, C. Wang, The Connection between flow pattern evolution and vibration in 90-degree pipeline: bidirectional fluid-structure interaction, Energy Sci. Eng. 10 (2) (2022) 308–323, https://doi.org/10.1002/ese3.1031.
[53] C. Kun, Z. Jianrong, C. Yilin, Q. Jie, Z. Changfan, Q. Jian, Z. Mingguang, Vibration cause analysis and elimination of stagnant branch pipeline, Eng. Fail. Anal. 141 (2022) 106666, https://doi.org/10.1016/j.engfailanal.2022.106666.
[54] G. Liu, L. Xu, J. Li, Q. Sun, Z. Liu, H. Chen, Simulation of abrasion characteristics of polar ship seawater pipelines under the coupling of ice particles and vibration, Appl. Sci-Basel. 10 (4) (2020) 1349, https://doi.org/10.3390/app10041349.